Strontium isotope stratigraphy of the Cretaceous

John M. McArthur* and Richard J. Howarth
Earth Sciences, University College London, Gower Street, London WC1E 6BT
JMM, 0000-0003-1461-7805
*Correspondence: j.mcarthur@ucl.ac.uk

Abstract: This contribution outlines the methodology of strontium isotope stratigraphy, and reviews the information that underpins the calibration curve of marine-$^{87}Sr/^{86}Sr$ against time for the Cretaceous.

When marine minerals, such as calcite, aragonite, gypsum, barite or apatite, precipitate from seawater they incorporate into their structure some of the strontium (Sr) dissolved in seawater. That Sr records the $^{87}Sr/^{86}Sr$ value of dissolved Sr at the time of incorporation. As the $^{87}Sr/^{86}Sr$ of Sr in the oceans has varied through Cretaceous time (Fig. 1), the numerical age of a marine mineral can be found by comparing its $^{87}Sr/^{86}Sr$ to the calibration curve, i.e. Figure 1, either in its graphical or tabular form. The tabular form is termed LOWESS 7 and is available from the senior author and from ResearchGate.

Values of $^{87}Sr/^{86}Sr$ can also be used to correlate different sections by comparing their profiles of $^{87}Sr/^{86}Sr$ against stratigraphic level (Fig. 2); levels correlate if they have the same $^{87}Sr/^{86}Sr$ value. The Sr-isotope ratio can be thought of as a proxy fossil (say, *Strontianus atomicus*) that has a measureable characteristic, $^{87}Sr/^{86}Sr$, which changes with time.

The method of dating and correlating rocks with $^{87}Sr/^{86}Sr$, outlined above, is termed strontium isotope stratigraphy (SIS hereafter). Since its proposal as a dating method by Wickman (1948), numerous workers have contributed data to the construction of the Cretaceous calibration curve of $^{87}Sr/^{86}Sr$ against time (*inter alia*, Peterman *et al.* 1970; Dasch and Biscaye 1971; Veizer and Compston 1974; Koepnick *et al.* 1985; McArthur *et al.* 1993*a*, *b*, 2007, 2020*a*; Jones *et al.* 1994*a*; Bralower *et al.* 1997; Veizer *et al.* 1997, 1999; Denison *et al.* 2003) and the trend of $^{87}Sr/^{86}Sr$ through Cretaceous time (some with, some without, accompanying data) have been provided by, *inter alia*, Burke *et al.* (1982), Smalley *et al.* (1994), Veizer *et al.* (1999), Prokoph *et al.* (2008) and McArthur *et al.* (2020*b*). The theory and practice of SIS is reviewed, *inter alia*, by Veizer (1989), Kuznetsov *et al.* (2018) and McArthur *et al.* (2020*b*).

This contribution focuses on SIS for Cretaceous time, so it updates, and adds detail to, the account of SIS given in McArthur *et al.* (2020*b*). That account shows the trend of $^{87}Sr/^{86}Sr$ against time for the past 3.8 Ga together with a tabulation (Excel tables) for Phanerozoic time (termed LOWESS 6) of age against $^{87}Sr/^{86}Sr$, and vice versa. Despite the narrow focus of this article, it is worthwhile summarizing some of the important points relevant to SIS, so these are outlined below.

What is '$^{87}Sr/^{86}Sr$'?

Measurements of $^{87}Sr/^{86}Sr$ of Sr in a sample are not measurements of the isotopic ratios of ^{87}Sr to ^{86}Sr in that sample; they are measurements of $^{87}Sr/^{86}Sr$ in the sample after adjustment of the ratio so that the sample's $^{86}Sr/^{88}Sr$ is 0.1194 (Thirlwall 1991). To explain, the isotopes of Sr fractionate in nature, but they also fractionate both during sample processing (to separate Sr from the sample matrix by ion-exchange chromatography) and during the mass-spectrometric analysis of Sr. In order to remove the fractionation arising during processing and measurement, isotopic ratios are corrected for that fractionation (Thirlwall 1991) and brought to a common basis of 0.1194 for the $^{86}Sr/^{88}Sr$ ratio. This process removes any natural fractionation of the isotopes that had occurred in nature. It is possible to measure the real $^{87}Sr/^{86}Sr$ of a sample, but the process involves a double-spike and two measurements on the same sample, so is seldom done; see Krabbenhöft *et al.* (2009) and Vollstaedt *et al.* (2014) for details.

The shape of the curve

The calibration curve in Figure 1 shows considerable sinuosity. Explanations of that sinuosity are beyond the remit of this article, so brief comments only on the matter are in order. The major variations (e.g. the late Aptian minimum) have been traditionally viewed as responses to changes in the flux and $^{87}Sr/^{86}Sr$ of three sources of Sr to the ocean: that from continental weathering (rivers and submarine

From: Hart, M. B., Batenburg, S. J., Huber, B. T., Price, G. D., Thibault, N., Wagreich, M. and Walaszczyk, I. (eds) *Cretaceous Project 200 Volume 1: the Cretaceous World*. Geological Society, London, Special Publications, **544**,
https://doi.org/10.1144/SP544-2023-85

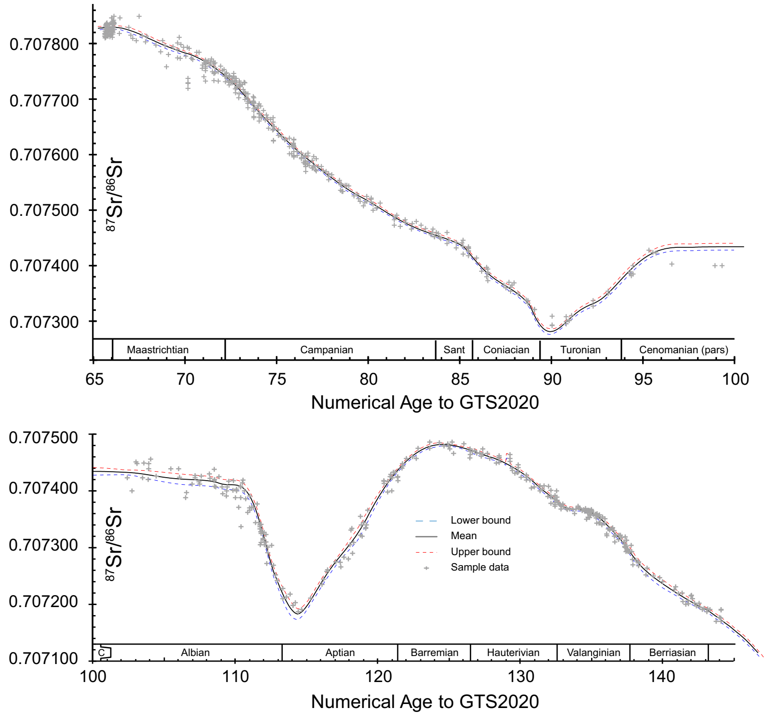

Fig. 1. The record of marine-$^{87}Sr/^{86}Sr$ through the Cretaceous. Age boundaries, and most of the rest of the timescale, are those of Gradstein *et al.* (2020), slightly modified within Ages in places identified in the text. A digitised version of the curve, as an Excel table termed LOWESS 7, accompanies this article. Source: updated from McArthur *et al.* (2020*b*).

groundwater discharge), with an $^{87}Sr/^{86}Sr$ around 0.710 (averaged globally; Peucker-Ehrenbrink and Fiske 2019); that from hydrothermal discharges at mid-ocean ridges (Spooner 1976 and many subsequent publications), which typically inputs to the ocean Sr with an $^{87}Sr/^{86}Sr$ of around 0.704 (Diehl and Bach 2023); that from carbonates deposited on the seafloor, and buried beneath it, that lose Sr to pore water (and, ultimately, seawater) during recrystallization, contributing Sr with a ratio that depends on the average age of that carbonate. This last flux is typically viewed as a minor influence. The magnitude of these fluxes, and their $^{87}Sr/^{86}Sr$ values, will have varied through time, thus causing the fluctuations in marine-$^{87}Sr/^{86}Sr$ seen in Figure 1. The present understanding regarding fluxes and their ratios is discussed in Coogan and Dosso (2015) and Peucker-Ehrenbrink and Fiske (2019).

The minor variations in the shape of the calibration curve, for example, the upward convexity of the Valanginian part of the curve, and the changes in gradient of the curve at the Coniacian–Santonian and the Campanian–Maastrichtian boundaries, may be real or may be artefacts of the age models used to construct the curve, perhaps because those age models do not adequately account for changes in sedimentation rate (cf. Fig. 3). Resolving such issues requires profiling $^{87}Sr/^{86}Sr$ through many more sections than has presently been done.

Age models

Calibration curves (e.g. Fig. 1) are made by assigning age models to trends of $^{87}Sr/^{86}Sr$ through rock sections. Age models need to be calibrated to an evolving geological timescale; here the primary calibration is to the numerical ages assigned to age/stage boundaries in the timescale of Gradstein *et al.* (2020, GTS2020 hereafter). Internal scaling between those boundaries is based mostly on zone boundaries in GTS2020, with alternative scaling for a few intervals that are detailed in the text.

Some principles that can guide the conversion of profiles of $^{87}Sr/^{86}Sr$ through rock into profiles of $^{87}Sr/^{86}Sr$ through time are outlined in Figure 3. Most of the Cretaceous calibration curve (Fig. 1) has been derived from sediments of nearshore settings and epeiric seas, which are commonly replete with condensed sections and hiatuses. The

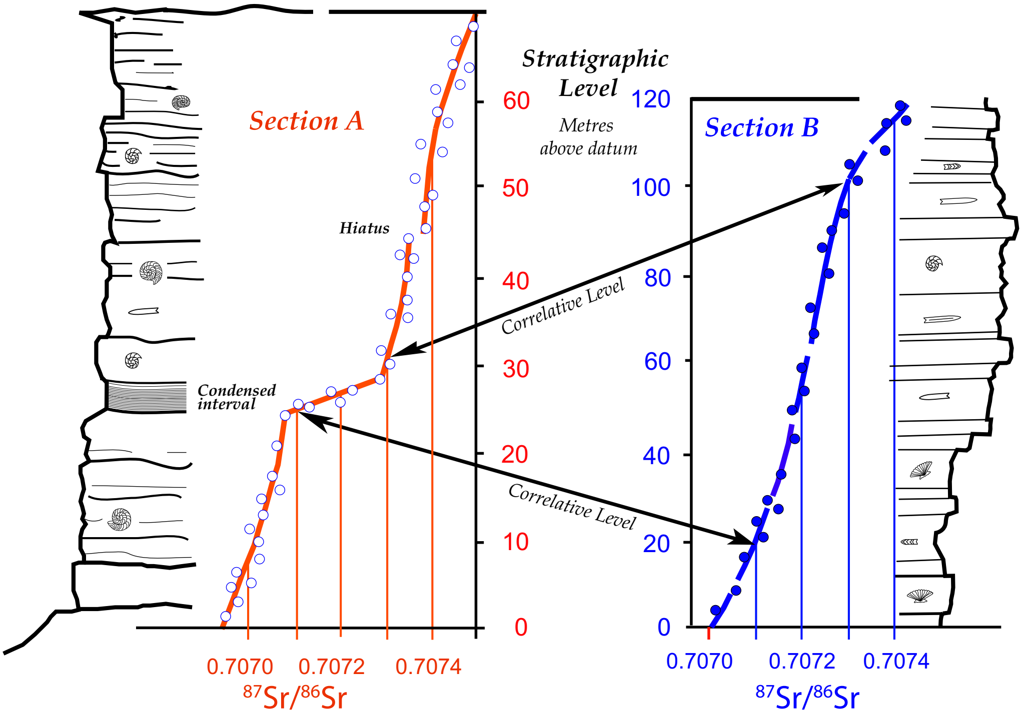

Fig. 2. Correlation with ^{87}Sr/^{86}Sr. Levels in marine sections anywhere in the world correlate when they have the same ^{87}Sr/^{86}Sr, provided the ^{87}Sr/^{86}Sr are measured accurately, corrected for interlaboratory bias, and obtained on well-preserved samples.

incompleteness of such stratigraphic records makes difficult the conversion of trends of ^{87}Sr/^{86}Sr against stratigraphic level ($\Delta R/\Delta L$, which is what is measured) into trends of ^{87}Sr/^{86}Sr against time ($\Delta R/\Delta t$, which is what is desired), so the process requires close attention to the difference between rock and time (e.g. Ager 1973, 1993; Sadler 1981; Barefoot *et al.* 2023; and references therein). Rock and time are sometimes confused: for example, a sudden increase in the slope of a profile of ^{87}Sr/^{86}Sr against stratigraphic level through a rock section has been described as a change to a more *rapid* rate of change of ^{87}Sr/^{86}Sr, thereby implying a faster $\Delta R/\Delta t$, when the changes expresses nothing more than a decrease in sedimentation rate (Figs 2 and 3).

A robust calibration curve of ^{87}Sr/^{86}Sr against time for any section can be obtained only when an accurate age model is available for that section. Age models for deep-sea cores constructed by cyclostratigraphy have often proven excellent (see, e.g. references in Westerhold *et al.* 2020). Attempts to use cyclostratigraphy to construct age models for sediment deposited beneath shelf seas and epeiric seas have been less successful (Bailey and Smith 2008*a*, b; Vaughan *et al.* 2011, 2014; Ruebsam *et al.* 2014, 2015; Weedon 2022; Smith 2023, Bailey 2023), or plainly wrong, because the commonly episodic deposition and variable rates of sedimentation in such environments is frequently overlooked (Ager 1973, 1993; Sadler 1981; Barefoot *et al.* 2023; see also Pearce *et al.* 2020 for a local study of changing sedimentation rates through time in the Chalk of the UK). The difficulty of incorporating such matters into cyclostratigraphic analysis are illustrated by, for example, the fact that cyclostratigraphic durations of the Albian range from ≈7.2 Myr (Leandro *et al.* 2022) through ≈9.4 (Charbonnier *et al.* 2023) to 13.42 Myr (Huang *et al.* 2010).

The best way to ameliorate the shortcomings of age models underpinning SIS is to profile ^{87}Sr/^{86}Sr against stratigraphic level through sections from widely separated locations. The one which gives the smoothest trend through the rock section is likely to be the one which best approximates the trend of ^{87}Sr/^{86}Sr through time.

Legacy data

It is often difficult to update legacy data for ^{87}Sr/^{86}Sr to evolving biostratigraphies and an evolving timescale. The ratification of GSSPs for 9 of the 12 Stages

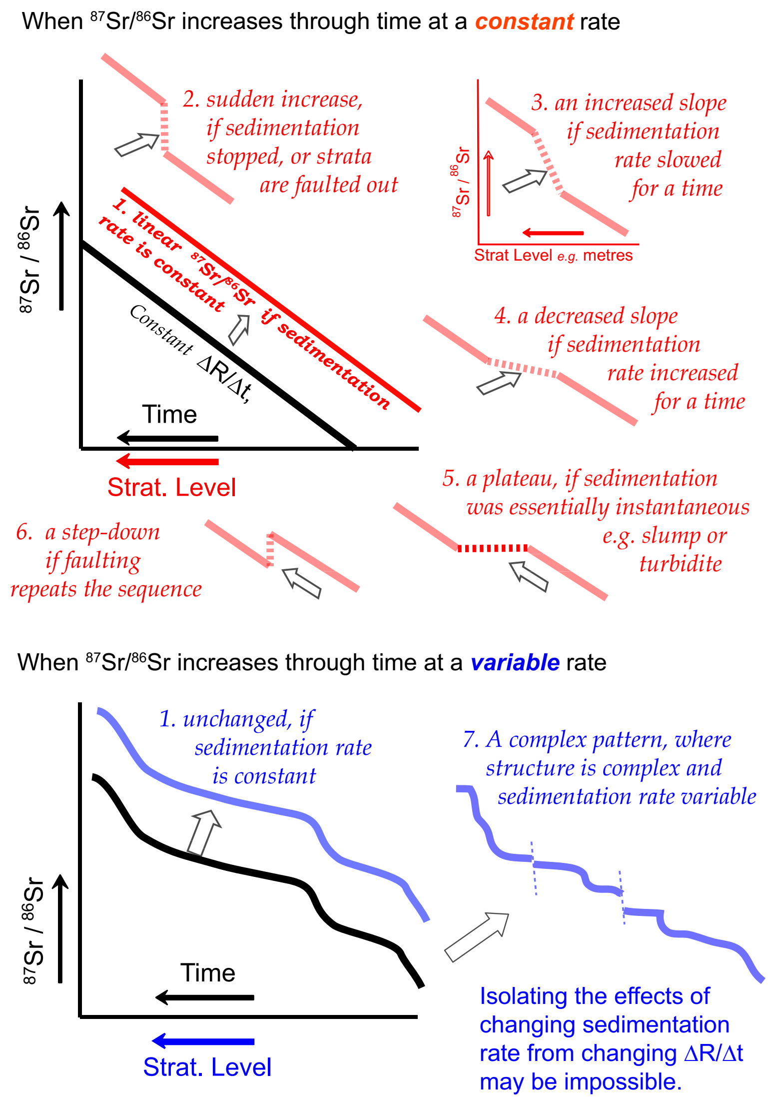

Fig. 3. The effect of changes in sedimentation rate on profiles of $^{87}Sr/^{86}Sr$ through a rock section. Rates of change of $^{87}Sr/^{86}Sr$ with stratigraphic level ($\Delta R/\Delta L$) must not be confused with rates of change of $^{87}Sr/^{86}Sr$ with time ($\Delta R/\Delta t$).

of the Cretaceous (the Berriasian, Valanginian and Aptian apart) has helped to stabilize some biostratigraphic nomenclature. Nevertheless, updating calibration curves is made difficult by continuing revision of zonal hierarchies, changes to fossil names, new fossil discoveries that force boundaries to move (usually) down in a section, and redefinitions of biostratigraphic boundaries. As an example, Reboulet *et al.* (2023) propose using ammonites as a boundary marker for the base of the Valanginian rather than the commonly used calpionelids and setting the boundary 7 m lower than previously accepted. As another example, the base of the Campanian has traditionally been set at the last occurrence of the crinoid *Marsupites testudinarius* (Gale *et al.* 1995), at which level the value of $^{87}Sr/^{86}Sr$ given by those authors was 0.707473 ± 0.000005 (2 s.e.). That boundary definition, and its $^{87}Sr/^{86}Sr$ value, are no longer relevant as the base of the Campanian is now set at the base of magnetic polarity Chron C33r (Gale *et al.* 2023), which causes a problem for SIS as none of the sections profiled for $^{87}Sr/^{86}Sr$ has a useful magnetic record (but see the later section on the Campanian). The curve presented in Figure 1 therefore represents only the authors' best efforts to accommodate such changes, and to deal with sometimes conflicting data, which occasionally involves a subjective choice, e.g. whether to constrain the Albian trend in $^{87}Sr/^{86}Sr$ by using the inoceramid data of Bralower *et al.* (1997) or the data of Denison *et al.* (2003).

Accuracy and precision of analysis

Using SIS to obtain reliable numerical ages, or to accomplish good biostratigraphic correlation, requires that close attention is paid to the accuracy and precision of analysis for $^{87}Sr/^{86}Sr$. The best modern instrumentation, used together with replicate analysis in order to reduce the standard error of the mean, allows $^{87}Sr/^{86}Sr$ to be measured today to a precision no better than ± 0.000001. The accuracy is unlikely to be better than ± 0.000004 owing to interlaboratory bias (Hildreth and Henderson 1971; McArthur 1994; McArthur *et al.* 2020*b*), a matter explained below.

Analysis of $^{87}Sr/^{86}Sr$ is done after extraction from the sample of the target Sr and purification of the Sr by ion-exchange chromatography. Traces of Rb may survive the purification process and be present during the measurement process. Rubidium has two isotopes, ^{85}Rb and ^{87}Rb, the latter indistinguishable from ^{87}Sr during conventional mass spectrometry. Correction is thus needed for this isobaric interference (see Thirlwall 1991 for the procedure for TIMS analysis). As an alternative possible during TIMS analysis, data acquisition for Sr can be delayed until all the Rb has been lost from the sample (Zaky *et al.* 2019), as analysis involves evaporating the purified sample at temperatures around 1400°C, during which Rb evaporates much faster than does Sr.

In order to have comparable measurements of $^{87}Sr/^{86}Sr$ between laboratories, measurement bias between them (interlaboratory bias) must be corrected for. Data must be adjusted (i.e. normalized) to an accepted value for the same standard, which is analysed in each laboratory. Two standards in common use are NIST987 (also termed SRM987), an $SrCO_3$ powder available from the National Institute of Standards and Technology, USA, with a value of 0.710248, and EN-1, a giant clam from Enewetak Atoll, distributed by the US Geological Survey, with a value recommended here of 0.709174 (Table 1); all data used in this work are normalized to these relative values. An older standard, a $SrCO_3$ made by Eimer and Amend Company of New York (Hildreth and Henderson 1971) has a value of 0.708022 $\pm$ 0.000004 (2 s.e., $n = 34$; Jones *et al.* 1994*b*) relative to 0.710248 for NIST(SRM)987. The E&A standard is not widely available. The use of IAPSO North Atlantic seawater as a standard is not recommended as it is stored in glass (risking contamination) and recent data (Mokadem *et al.* 2015; reinterpreted in fig. 7.6 of McArthur *et al.* 2020*b*) hints that open-ocean seawater is not uniform in its $^{87}Sr/^{86}Sr$ composition. A modern coral, JCp-1, primarily used as a standard for Sr/Ca measurements, is occasionally used to represent modern marine $^{87}Sr/^{86}Sr$. It was distributed by the Geological Survey of Japan but is no longer exported from Japan. Finally, an alternative to EN-1 is to use modern shells from open-ocean environments away from rivers. This route requires checking for non-marine influences on $^{87}Sr/^{86}Sr$. For example, use of oysters, which can live in brackish environments, is not recommended unless the provenance is known definitively to be fully marine (see the next section for details).

Interlaboratory bias is supposedly corrected for by measuring $^{87}Sr/^{86}Sr$ in a standard, calculating the difference between measured and accepted values, and then adding that difference to all data (e.g. if a laboratory reports 0.710258 for SRM987, then −0.000010 should be added to all data that lab produces). In theory, which standard is used should not matter. Unfortunately, the differences *between* the values of standards (i.e. the $^{87}Sr/^{86}Sr$ of SRM987 minus the $^{87}Sr/^{86}Sr$ of EN-1 or similar) are not the same for every laboratory (Hildreth and Henderson 1971; McArthur 1994; Table 1): data for a laboratory that normalizes data to SRM(NIST)987 may therefore differ systematically from data obtained in a laboratory that normalizes data to EN-1 or an equivalent.

The standard used should be that which has an $^{87}Sr/^{86}Sr$ value that is closest to the values being measured. On that basis, use of E&A would be best for many deep-time studies because, of all available standards, its $^{87}Sr/^{86}Sr$ is nearer to the values measured in marine minerals. Unfortunately, E&A is not widely available, so normalization to EN-1 or an equivalent is the usual alternative even though all Cretaceous values of $^{87}Sr/^{86}Sr$ are well below its value of 0.709174.

As an example of the effect of interlaboratory bias, Figure 4 compares two trends in $^{87}Sr/^{86}Sr$ through Maastrichtian time. One trend is based on McArthur and Howarth (2004). The other trend is based on Huber *et al.* (2008), updated from MacLeod *et al.* (2003) for sediments from ODP cores from Blake Nose. Both trends are given to the same (outdated) timescale of Gradstein *et al.* (2004). During the Maastrichtian, $\Delta R/\Delta t$ was only +0.000020 per Myr. The trend through the data of MacLeod *et al.* (2003) is around 0.000018 higher than, but parallel to, the calibration curve of McArthur and Howarth (2004). The difference can be ascribed to interlaboratory bias. Were data from MacLeod *et al.* (2003) used to derive numerical age from Figure 1 without correction for that bias (i.e. without subtraction of

Table 1. Values of $^{87}Sr/^{86}Sr$ in EN-1, seawater and modern marine biogenic carbonate. All values adjusted to a value of 0.710 248 for SRM(NIST)987.

No.	Standard	Value	2 s.e × 10^6	*n*	Author
1	E&A	0.708 022	1	34	Jones *et al.* (1994*a*)
2	EN-1	0.709 185			Hodell *et al.* (1990)
3	Foraminifera	0.709 187	9	11	Hodell *et al.* (1990)
4	Foraminifera	0.709 187	9	11	Hodell *et al.* (1990)
5	EN-1	0.709 166	2	348	Zaky *et al.* (2019)
6	EN-1	0.709 161	4	24	Zaky *et al.* (2019)
7	Foaminifera	0.709 173	1	10	Henderson *et al.* (1994)
8	Foraminifera	0.709 175	3	8	Farrell *et al.* (1995)
9	Corals <10 ka	0.709 174	2	27	Ando *et al.* (2010)
10	Foraminifera	0.709 175	3	12	Ando *et al.* (2010)
11	EN-1	0.709 174	2	37	McArthur (2010)
12	EN-1 (2004/5)	0.709 177	2	17	Kuznetsov *et al.* (2012)
13	EN-1 (2009/10)	0.709 175	1	26	Kuznetsov *et al.* (2012)
14	Modern shells	0.709 175	1	49	Kuznetsov *et al.* (2012)
15	JCp-1	0.709 172	4	32	Vollstaedt *et al.* (2014)
16	Modern shells	0.709 173	7	13	Vollstaedt *et al.* (2014)
17	Seawater	0.709 172	1	17	Mokadem *et al.* (2015)
18	Foraminifera	0.709 171	1	11	Mokadem *et al.* (2015)
19	JCp-1	0.709 170	6	10	Voigt *et al.* (2015)
20	EN-1	0.709 171	2	26	Dudás *et al.* (2017)
21	Modern shells	0.709 172	1	31	El Meknassi *et al.* (2018)
22	Modern shells	0.709 168	2	24	Farkaš *et al.* (2018)
23	Core top	0.709 171	6	13	Matsui *et al.* (2019)
24	EN-1	0.709 170	0.6	195	Paces *et al.* (2023)
	Recommended value	**0.709 174**			

5. Long-term average, Bochum University
6. Study average for Zaky et al. (2019)
7. Mean of samples <31 ka
8. Mean of samples <50 ka
9. Ages by radiocarbon, mean of samples <30 ka
10. Mean of samples <25 ka
18. Mean of samples <44 ka, ODP Site 758A
21. Modern biogenic carbonate, unrestricted Atlantic and Pacific coasts; 31 analyses of 31 samples
23. Extrapolated to 0 mbsf
24. For five-year period

0.000018 from their data), the error in a predicted age would be 0.9 Myr.

Few of the analyses used for the construction of the calibration curve in Figure 1 attained precision below ±0.000015, as do few of the analyses used by other authors for dating by SIS. If SIS is to realize its full potential to date and correlate marine sediments, the calibration curve shown in Figure 1 needs to be reconstructed from scratch, using the best modern instrumentation and samples from well-documented and stable sites where $^{87}Sr/^{86}Sr$ values can be tied directly to place-in-section, so that changing biostratigraphies can be accommodated.

Homogeneity of marine-$^{87}Sr/^{86}Sr$

SIS is based on the assumption that the oceans have always been homogeneous with respect to $^{87}Sr/^{86}Sr$. The degree to which this was true depends on the accuracy with which $^{87}Sr/^{86}Sr$ is measured. As rivers, submarine groundwater discharge, and mid-ocean-ridge hydrothermal plumes, have $^{87}Sr/^{86}Sr$ different from that of open-ocean seawater, any mix will have an $^{87}Sr/^{86}Sr$ reflecting the relative proportions of that mix. Such mixing was modelled or discussed by, *inter alia*, Ingram and Sloan (1992), Andersson *et al.* (1992), McArthur *et al.* (1994, 2020*b*), Bryant *et al.* (1995), Kuznetsov *et al.* (2012), El Meknassi *et al.* (2018) and Zaky *et al.* (2019): Kuznetsov *et al.* (2012) demonstrate particularly well the departures from 0.709174 of $^{87}Sr/^{86}Sr$ in samples from closed and semi-closed basins, such as the Sea of Azov.

The problem posed by riverine influences increases as the accuracy and precision of measurement of $^{87}Sr/^{86}Sr$ increases (Fig. 5). At the best

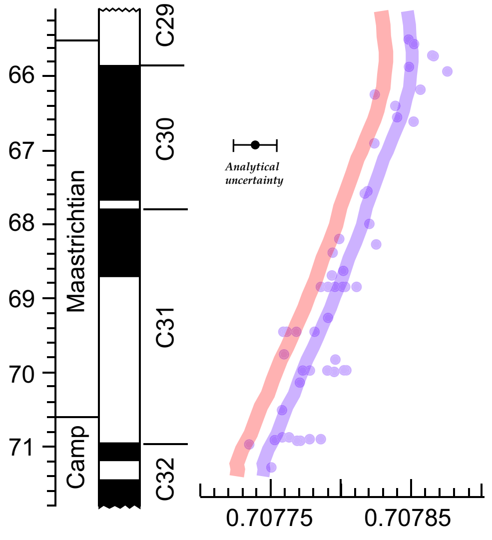

Fig. 4. The effect of interlaboratory bias on numerical ages derived by SIS. The pink trend (for clarity, shown without data) is the $^{87}Sr/^{86}Sr$ calibration curve of McArthur and Howarth (2004). The blue trend, with data points, is the preferred trend of Huber *et al.* (2008) through the data of MacLeod *et al.* (2003) for ODP cores from Blake Nose. Both trends are to the timescale of Gradstein *et al.* (2004). Compared to the pink calibration curve, the blue trend is higher by 0.000 018. See the text for an interpretation of the difference in $^{87}Sr/^{86}Sr$ between the trends.

attainable precision of ± 0.000001, 87% of modern rivers can alter the $^{87}Sr/^{86}Sr$ of seawater at a dilution of 15%, i.e. from a salinity 35 psu to one of 30 psu (Fig. 5): at a precision of ± 0.000020, typical of many analyses, as many as 10% can do so. Whilst such non-marine influences pose a problem for SIS, the problem may be over-emphasized because it is not always clear what part of the range of $^{87}Sr/^{86}Sr$ for modern marine Sr in some reports arises from real heterogeneity and what arise from artefacts of preservation, analysis, or normalization.

When using SIS, non-marine influences should be looked for palaeontologically. When that is not diagnostic, such influences might be detectable by analysing specimens from both benthic and planktic environments from a single stratigraphic level, or multiple specimens of the same species from a single stratigraphic level. If variation in measured values of $^{87}Sr/^{87}Sr$ is greater than analytical precision, either non-marine influences or imperfect preservation is indicated (on the latter, see later).

Samples for SIS

Samples analysed for SIS in the Cretaceous are usually belemnites and brachiopods as these are common in Cretaceous sediments and often preserve their original signals well, albeit only in resistant parts of the fossil. Notwithstanding that, most well-preserved marine precipitates will serve, e.g. gypsum, apatite (conodonts, shark teeth), barite and carbonate cements. Care is needed when dating gypsum (and anhydrite) as freshwater influences may have been strong in evaporites and lead to erroneous dates: Denison *et al.* (1998) and Denison and Peryt (2009) discuss and illustrate the problem well. Biogenic phosphate (e.g. shark teeth) tends to be altered diagenetically (Martin and Scher 2004) and seldom gives accurate results for SIS, although it often yields approximate ages that are, nevertheless, useful. Analysing bulk carbonate sediment risks contamination from Sr derived from diagenetic and clastic phases, thus skewing the result. Contamination from clastics often increases $^{87}Sr/^{86}Sr$ in samples from continental settings and decreases $^{87}Sr/^{86}Sr$ in samples from settings with mantle affinity (e.g. back-arc basins).

Where analysis of bulk sediment is the only option, it should be used only on samples that contain little detrital material. The meaning of the term ‘little’ needs to be decided on a case-by-case basis, but more than 2% detrital material is likely to create contamination from non-target phases of a magnitude that exceeds analytical uncertainty. The likelihood of getting good data from whole-rock analysis is hypothesized here to be inversely proportion to the degree of lithification of a sample. Ways to minimize, but not eliminate, contamination when analysing bulk sediment are given in Bailey *et al.* (2000) and McArthur *et al.* (2020*b*). In brief, use gentle dissolution methods, such as 90% acetic acid, and use a serial leaching process to remove as much contaminant as possible and target the most unaltered part of the sample.

Sample preservation

Use of SIS requires well-preserved samples and that, in turn, requires assessment of the quality of preservation of the material analysed (usually biogenic calcite). Samples are typically described in published works as ‘well preserved’. Whether they are so is often debatable. The term ‘well-preserved’ is subjective and interpreted differently by palaeontologists and geochemists. Here, the term ‘well preserved’ means that samples retain their original $^{87}Sr/^{86}Sr$ value. Multiple criteria exist for assessing preservational state. Most commonly used is the content of Sr, Fe and Mn (Brand and Veizer 1980, 1981; Veizer 1989; Podlaha *et al.* 1998; amongst others) but for reservations on the use of Fe and Mn, see Jones *et al.* (1994*a*, *b*). The concentration of Ba in calcite may signal alteration if present at concentrations >10 ppm (Li *et al.* 2021); the advantage of Ba

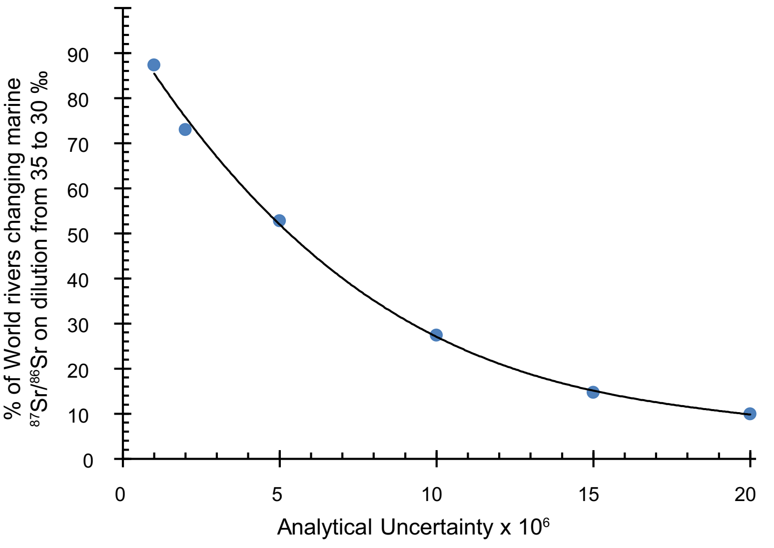

Fig. 5. How rivers influence marine-$^{87}Sr/^{86}Sr$. The graph shows the percentage of world rivers that can alter the $^{87}Sr/^{86}Sr$ of ocean water, of salinity 35 ‰, on dilution by river water to a salinity of 30 ‰, as a function of the analytical uncertainty of measurement. The data fit a third-order polynomial, where (% of rivers affected) = $-0.008390783958683870P^3 + 0.5106333093901980P^2 - 11.17168323666120P + 96.10179076199820$, and P = analytical precision. Source: based on data for 252 rivers compiled in Goldstein and Jacobsen (1987), Palmer and Edmond (1989), Pearce *et al.* (2015), Peucker-Ehrenbrink (2009, 2018) and Peucker-Ehrenbrink and Fiske (2019).

over Mn and Fe is that Ba is not redox-sensitive. Cathodoluminescence is excellent at assessing alteration in calcite (Marshall 1988 and many later papers on this topic), but it is not foolproof as some modern biogenic carbonate (presumably unaltered) shows luminescence (Barbin *et al.* 1991). Another excellent method is visual inspection, in both hand specimens and as fragmented samples under the binocular microscope (Fig. 6), and as polished and/or thin section (Li *et al.* 2021; fig. 7.8 of McArthur *et al.* 2020*b*). For calcite, visual inspection and cathodoluminescence are better than trace-element analysis as they are more sensitive to small degrees of alteration. For aragonite, scanning electron microscopy is often used but is not diagnostic unless used at magnifications of at least 20 000, since that degree of magnification is needed to see variable thickness in nacre layers, and overgrowths on nacre plates (Fig. 6g, h).

An excellent test of preservation is to compare the precisions, as standard deviations, of sample data, replicate data on individual samples and standards run with samples (e.g. Jones *et al.* 1994*b*). Neither the precision of replicates of a single sample, nor the precision (of detrended) sample data, should be greater than the precision of analysis of the data as judged by multiple analysis of standards. As an example, Jones *et al.* (1994*b*) provided 28 analyses of 12 belemnites from a single bedding plane; only one sample departed from the mean value of all analyses by more than analytical uncertainty (± 0.000025, 2.s.d.), so only one sample could be considered altered (Fig. 7a). As another example, McArthur *et al.* (2004) provided 32 analyses, with a precision of ± 0.000015 (2.s.d.; incorrectly reported as 2 s.e. in that paper), for 15 belemnites from 2.4 m of the Valanginian *Polyptichytes* Beds of Speeton, UK. The data show no overall trend (i.e. $\Delta R/\Delta L = 0$; Fig. 7b) and residuals about a line of linear regression are $\leq \pm$ 0.000014, with all but one being $\leq \pm$ 0.000010. On this basis, the samples were well preserved.

Corrections for ^{87}Rb decay

The incorporation of marine Sr into a mineral is accompanied by the incorporation of marine Rb. Atoms of ^{87}Rb decay to ^{86}Sr and so can alter the $^{87}Sr/^{86}Sr$ of a mineral, potentially leading to a false age derived from SIS. Whether correction is needed depends on the Sr/Rb of the sample and its age.

From theory, for Cretacous samples, correction for Rb decay is needed only if the precision sought is $\leq$0.000001 and Sr/Rb is less than 7000 (for a more detailed discussion of this topic, see table 7.2 of McArthur *et al.* 2020*b*). How likely is it that Sr/Rb mass ratios <7000 will be encountered in

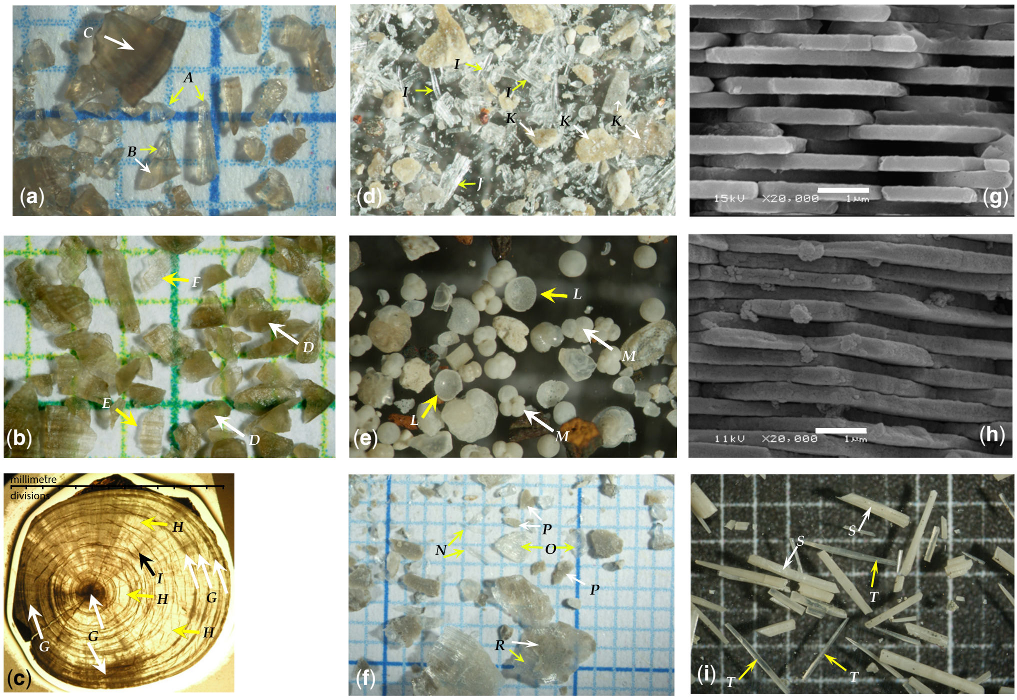

Fig. 6. Photographs of fragmented fossils assessed for use in SIS. White arrows indicate some of the altered parts, yellow arrows indicate some of the well-preserved parts. The smaller squares are 1 mm on a side. (**a**) A fragmented Toarcian belemnite from Peniche, Portugal: A, fragments of clear, pristine, calcite with a strong radial fabric; B, a triangular fragment in which only the upper 30% is well preserved – the horizontal black band is interpreted to be organic matter or pyrite (or both); C, a large fragment of cloudy, altered, calcite from close to the belemnite exterior. (**b**) A fragmented Valanginian belemnite from Vergol, southeastern France, showing fragments with a range of preservation from mostly poor (D) through acceptable (E) to good (F). The middle third of the fragment at E (between the alteration bands) could be isolated for analysis. Despite the occurrence of rare good fragments, this sample was rejected for use in SIS. (**c**) Thin section of a Toarcian belemnite (V9 of McArthur *et al.* 2007) showing cloudy altered calcite (G) in the west and south of the specimen, in the apical area, and along prominent alteration bands (often erroneously termed ‘growth bands’) and areas of clear unaltered calcite (H). Dark irregular lines (e.g. at I; black arrow) are fractures induced in preparation of the thin section. (**d**) Brachiopod, Aalenian. Mostly well-preserved acicular calcite as individual laths (I) or aggregates of laths (J) amongst many altered calcite fragments (K). (**e**) Pliocene foraminifera from, Punta Piccola, Sicily, showing a range of preservational states from excellent (glassy; L) to poor (frosty, M). (**f**) Fragmented Toarcian brachiopod from Peniche (sample 9.65 m of Li *et al.* 2021). N, two laths of clear, pristine, calcite. O, aggregated sheets of bundled crystallites of clear, pristine calcite. P, thoroughly altered calcite. R, double layer of sheeted laths; the upper layer shows surface contamination and alteration and the underlying layer is pristine. (**g**) Well-preserved aragonite from a Campanian specimen of *Baculites obtusus* from the Pierre Shale, US Western Interior (sample 96 of McArthur *et al.* 1994). Note the fairly uniform platelet thickness and lack of overgrowths and absence of knobbly surfaces on the platelets. Scale bar = 1 micron. (**h**) Poor preservation in a Campanian specimen of *Baculites cuneatus*, Pierre Shale, US Western Interior (sample 16 of McArthur *et al.* 1994). Note the woolly appearance of plate surfaces, their rounded edges and uneven thickness of plates, all of which signal alteration. This sample gave an anomalous value of $Sr/^{86}Sr$. Scale bar = 1 micron. (**i**) Disaggregated calcite prisms of a giant inoceramid, Coniacian, Antarctic Peninsula; most prisms are opaque and altered (S), but a few (T) have clear portions of unaltered calcite that are separable for analysis.

samples for SIS? Data for Rb in calcite are uncommon: Kiel *et al.* (2014) report concentrations of Rb <0.03 ppm (Sr/Rb ≈ 10 000) in Cretaceous specimens of the rhynchonellid brachiopod *Peregrinella*, whilst McArthur *et al.* (2000) report Rb concentrations typically <0.1 ppm in Toarcian belemnite calcite (Sr/Rb >15 000). Given such sparse data, we additionally use a proxy argument to evaluate the likelihood of a Rb problem affecting Cretaceous samples. The size of the Rb^{+} ion is larger than the size of the Ca^{++} ion (161 *v.* 112 pm at CN = 8; Speight 2017) so aragonite, in which the cation site

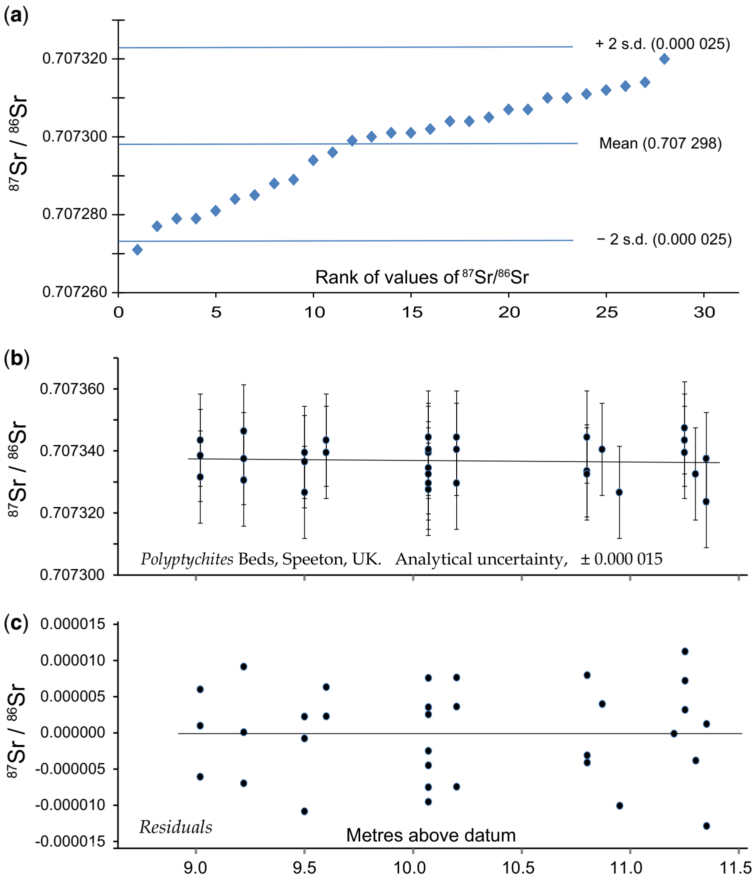

Fig. 7. (**a**) Ranked $^{87}Sr/^{86}Sr$ values for 28 analyses of 12 belemnites from a single stratigraphic horizon, together with uncertainty limits of 2 s.d. on the analysis. (**b**) Profile on $^{87}Sr/^{86}Sr$ through 2.4 m of the hiatus-bound *Polyptychites* Beds of the Speeton Clay at Speeton, Yorkshire, UK. Horizontal line is a linear regression fit to the data. (**c**) the regression residuals and a linear trend fitted to them. Source: (a) data of Jones *et al.* (1994*b*); (c) data of McArthur *et al.* (2004).

is larger than in calcite, should incorporate more Rb than does calcite. Yet Sr/Rb in aragonite is >9000 in coralline aragonite (Allison 1996) and >49 000 in inorganic marine aragonite (Oyanagi *et al.* 2021). From all of the above, Sr/Rb mass ratios <7000 are unlikely to occur in Cretaceous carbonates used for SIS. Information is lacking on the Rb content of gypsum, anhydrite, barite or biogenic apatite, so analysis for Rb would be wise when dating such materials by SIS.

Notes on the calibration curve (Fig. 1)

Berriasian, 143.1 ± 0.6

No formal GSSP has been fixed for the base of the Berriasian Stage (ICS 2023). The base of the Stage is here set at the level set in GTS2020, which is at the level of the first appearance of the calpionelid *Calpionella alpina*, a level approximately in the middle of magnetochron M19n.2n. The numerical age assigned in GTS2020 is 143.1 Ma. The level correlates to the middle of the *Berriasella jacobi* ammonite Zone in western Tethys (GTS2020, fig. 27.9). The equivalent level on the Russian Platform is the base of the *Craspedites milkovensis* Sz. of the *Craspedites nodiger* ammonite Zone (upper Volgian; Wierzbowski *et al.* 2017). The base of the Berriasian has an $^{87}Sr/^{86}Sr$ of 0.707190 ± 0.000003 (2 s.e., $n = 23$) as defined by analysis of belemnites from the Boreal Realm (Kuznetsov *et al.* 2017), with minor contributing data from belemnites from southeastern France (McArthur *et al.* 2007). Upwards from the base of the Berriasian, $^{87}Sr/^{86}Sr$ appears to increase more or less linearly with time to the base of the Valanginian (Fig. 1).

Valanginian, 137.7 ± 0.5

No GSSP has been fixed for the base of the Valanginian Stage (ICS 2023). In view of that, the Tethyan base of the Valanginian is set here at the base of the '*Thurmanniceras*' *pertransiens* ammonite Zone at Vergol, in SW France (Kenjo *et al.* 2021), which is a candidate section and placement for the Valanginian GSSP (Reboulet *et al.* 2023). Owing to new finds of ammonites in sections at Vergol, the base set by Kenjo *et al.* (2021) is around 7 m lower than that recognized in the ^{87}Sr/^{86}Sr curve for the Valanginian given in McArthur *et al.* (2007). The new boundary profile at Vergol for ^{87}Sr/^{86}Sr is shown in Figure 8. The new boundary value is 0.707289 ± 0.000004 (2 s.e., $n = 12$), which is 0.000005 less than the value given in McArthur *et al.* (2007, 2020*b*). The base of the Boreal Valanginian (Ryazanian -Valanginian boundary) appears to be fixed by the data of Möller *et al.* (2015) at 0.707293 ± 0.000003 (2s.e., $n = 14$).

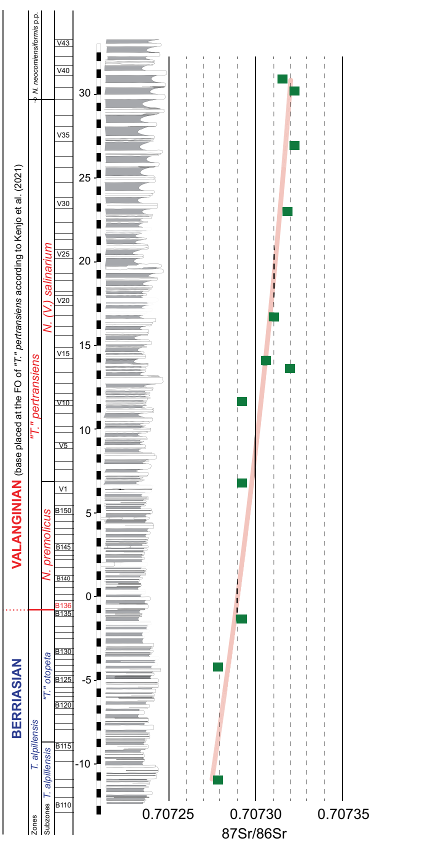

Fig. 8. Profile of ^{87}Sr/^{86}Sr through the Berriasian/Valanginian boundary section at Vergol, SE France. All samples are from the Vergol section. Source: litholog courtesy of S. Reboulet.

The Valanginian part of the calibration curve (Fig. 1) is based the ^{87}Sr/^{86}Sr of belemnites from sections in the Vocontian Basin of southeastern France (McArthur *et al.* 2007). The age model used is based on numerical ages of ammonite zones and subzones given in GTS2020: these, in turn, are based on the cyclostratigraphy of Martinez *et al.* (2013, 2015) for the limestone-marls alternations of the Vocontian Basin, southeastern France where, through the Valanginian and Hauterivian, age is approximately linearly related to stratigraphic level (Fig. 9). In the uppermost Valanginian, $\Delta R/\Delta t$ decreases in the middle Late Valanginian to essentially zero before increasing again across the Valanginian–Hauterivian boundary and continuing to increase through the Hauterivian. It remains to be seen if these Late Valanginian changes in $\Delta R/\Delta t$ are artefacts of an incorrect age model arising from changing rates of sedimentation, or whether they are real. The plot of ^{87}Sr/^{86}Sr against level shown for the Valanginian in Möller *et al.* (2015, their fig. 2; see also McArthur *et al.* 2016, fig. 9 and discussion) suggests that a more linear trend might be more appropriate; however, the data of the former for the Upper Valanginian are sparse so that interpretation is uncertain.

Hauterivian, 132.6 ± 0.6

The GSSP for the Hauterivian Stage is placed at the base of Bed 189 in the La Charce section of southeastern France (Mutterlose *et al.* 2021). This level marks the first occurrence of the ammonite genus *Acanthodiscus* which, in southeastern France, is the base of the *Acanthodiscus radiatus* ammonite

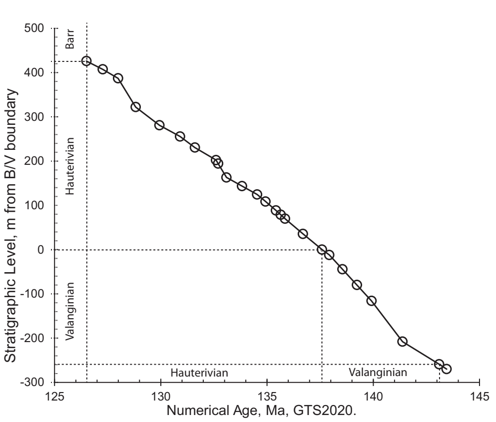

Fig. 9. Numerical ages of ammonite zones and subzones from GTS2020 plotted against stratigraphic level for the composite section for the Vocontian Basin, S.E. France, given in McArthur *et al.* (2007).

Zone. No profile exists of $^{87}Sr/^{86}Sr$ through the section at La Charce. The Valanginian–Hauterivian boundary profile of McArthur *et al.* (2007) is based on belemnites from Vergol and Angles, both also in southeastern France. Correlation of those sections to La Charce yields a value for the Valanginian–Hauterivian boundary of 0.707383 using the data of McArthur *et al.* (2007), with the 2 s.e. recalculated here to be $\pm$0.000 002 ($n = 9$).

In the UK, the lowest Hauterivian strata of the Speeton Clay is the *Endemoceras amblygonium* ammonite Zone, which marks the base of the Boreal Hauterivian (fig. 27.9 in GTS2020). The mean $^{87}Sr/^{86}Sr$ value of three measurements on belemnites from this zone is 0.707381 $\pm$ 0.000002 (range of three values; McArthur *et al.* 2004). The value of $^{87}Sr/^{86}Sr$ confirms that deposition of Hauterivian sediment at Speeton began in the earliest Hauterivian on a phosphatic remanié surface of Valanginian age (Rawson 1971). The $^{87}Sr/^{86}Sr$ values of belemnites from 2.4 m of the 3.8 m of the Boreal Valanginian sediments (most of the *Polyptychites* Beds, Fig. 7b) underlying the remanié surface is 0.707337 $\pm$ 0.000002 (2.s.e, $n = 32$). That ratio correlates to the boundary of the *biasselense*/*campylotoxus* Szs of the *B. Campylotoxus* Zone of the Tethyan Vocontian Basin (McArthur *et al.* 2007); the zonation of the Vocontian Basin has since been revised (Reboulet *et al.* 2023).

Barremian, 126.5 $\pm$ 0.7

The GSSP for the Barremian Stage is in the process of final approval but will be in Bed 171 in the section at Río Argos near Caravaca, Murcia Province, Spain at the first appearance of the Tethyan ammonite *Taveraidiscus hugii* (ICS 2023). No useful $^{87}Sr/^{86}Sr$ data exist for the section but extrapolation from sparse $^{87}Sr/^{86}Sr$ values for uppermost Hauterivian belemnites in correlative equivalents in the Tethyan Vocontian Basin (data in McArthur *et al.* 2007) suggest that the base of the *T. hugii* zone in Tethys has an $^{87}Sr/^{86}Sr$ value of 0.707474 $\pm$ 0.000010 (2 s.e., $n = 6$). The belemnite $^{87}Sr/^{86}Sr$ data of Bodin *et al.* (2015) for the Tethyan Vocontian Basin, predicts a value of 0.707472 $\pm$ 0.000005 (2 s.e., $n = 19$) for the base of the Barremian. The base of the Tethyan *T. hugii* ammonite Zone equates to the base of the Boreal *Paracrioceras rarocinctum* ammonite Zone (GTS2020). In the Boreal record of $^{87}Sr/^{86}Sr$, based on belemnites from the Speeton Clay, Yorkshire, UK (data of McArthur *et al.* 2004), the base of the *P. rarocinctum* Zone, and so the base of the Boreal Barremian, has an $^{87}Sr/^{86}Sr$ value of 0.707475 $\pm$ 0.000001 (2 s.e., $n = 16$).

A detailed record of $^{87}Sr/^{86}Sr$ through Barremian time was given in McArthur *et al.* (2004) for the Boreal Realm and was based on the Speeton Clay. That record formed the basis of the Barremian part of the Sr-isotope calibration curve in McArthur *et al.* (2020*b*; LOWESS 6). The numerous hiatuses in the Speeton Clay section, and the variable sedimentation rate through it, suggest that a better basis for a calibration curve for the Barremian is the sparser data of Bodin *et al.* (2015) for the Vocontian Basin, where sedimentation appears less interrupted, so the Barremian in Figure 1, and in the LOWESS 7 fit, was prepared on that basis.

The stratigraphic position of the Barremian maximum in $^{87}Sr/^{86}Sr$ is, however, poorly defined in the data of Bodin *et al.* (2015). At Speeton, for which data are more abundant, the maximum $^{87}Sr/^{86}Sr$ of 0.707485 $\pm$ 0.000003 (2 s.e. $n = 8$) occurs in the *Paracrioceras elegans* ammonite Zone which, according to figure 27.9 of GTS2020, correlates to the Tethyan ammonite zone of *Moutoniceras moutonianum*, with bounding ages for both of 124.4 and 124.8. Accordingly, LOWESS 7 has the Barremian maximum of 0.707485 at 124.8 Ma.

Aptian, 121.4 $\pm$ 0.6, and Albian, 113.2 $\pm$ 0.3

No GSSP for the Aptian Stage has been agreed (ICS 2023) but the base of magnetic anomaly M0r is typically used as a marker level for the base of the Stage (e.g. GTS2020). This level is around 0.2 Myr later than the first appearance of the ammonite *Deshayesites oglanensis* (GTS2020) The GSSP for the Albian Stage is set at 0.4 m above the base of the Niveau Kilian bed (a laminated shale) in the Vocontian Basin at Col de Pré-Guittard, Department Drôme, in southeastern France (Kennedy *et al.* 2017).

The trend of $^{87}Sr/^{86}Sr$ through the Aptian and Albian is based on four datasets. The first, that of Bodin *et al.* (2015) for belemnites from the Vocontian Basin, southeastern France, is calibrated by ammonite zones and is mostly for the Aptian. The second, that of Bralower *et al.* (1997) for inoceramid data for ODP Site 51, is calibrated to microfossil datums and it is mostly for the Albian. Here, the data of Bralower *et al.* (1997) are revised to the age model for Site 511 given by Dummann *et al.* (2020). The third is that of Jenkyns *et al.* (1995) for atoll carbonates from the Mid-Pacific Mountains (notably Resolution Guyot), for which age control is based on SIS because of a lack of age-diagnostic fossils; this dataset is used simply to provide qualitative confirmation of the trends from the other two sets of data. The last is that of Burla *et al.* (2009) for the Luz Section (Algarve Basin, Portugal) with weak biostratigraphic control but which confirms a late Aptian minimum, the level and $^{87}Sr/^{86}Sr$ value of which is probably not obscured by a hiatus between the

Lower and Upper Luz Marls because the minimum $^{87}Sr/^{86}Sr$ is within analytical uncertainty of the minimum value seen in other sections (discussed below). Sparse $^{87}Sr/^{86}Sr$ data, at two levels close to the Aptian–Albian boundary, given in Kennedy *et al.* (2000), are from multiple localities and difficult to place within the stratigraphic framework used here, so are not used.

The $^{87}Sr/^{86}Sr$ value for the base of the Aptian is around 0.707436 based on the data of Bodin *et al.* (2015). In the section at Cresmina (Lusitanian Basin, Portugal), a value of 0.707446 ± 0.000005 (2 s.e., $n = 14$) can be derived for the base of the Aptian from the data of Burla *et al.* (2009).

The base of the Albian has a value around 0.707227 based on the sparse Albian data of Bodin *et al.* (2015) and the more numerous data of Bralower *et al.* (1997).

In the Aptian–Albian interval, $^{87}Sr/^{86}Sr$ declines through the Aptian to a minimum in the latest Aptian, and an increase through the early Albian (Fig. 1). The minimum $^{87}Sr/^{86}Sr$ value recorded by Burla *et al.* (2009) is 0.707179 ± 0.000013 (2 s.e., $n =$ 3). The minimum $^{87}Sr/^{86}Sr$ recorded by Bralower *et al.* (1997), defined by two samples, is between 0.707211 and 0.707213, both with measurement uncertainty of ±0.00 0 025, whilst the minimum recorded by Bodin *et al.* (2015) is 0.707193 ± 0.000009 (2 s.e., $n = 6$). The biostratigraphic level of the latest Aptian minimum in $^{87}Sr/^{86}Sr$ differs between Bralower *et al.* (1997) and Bodin *et al.* (2015). In Bodin *et al.* (2015), from their figure 5, the minimum occurs between the Jacob Level and the higher Kilian Level, in the *Hypacanthoplites jacobi* ammonite Zone, around 35% up from its base (their fig. 5). According to Herrle and Mutterlose (2003, their fig. 5) this is within the lower part of nannofossil Zone NC8A of Roth (1978). In Bralower *et al.* (1997) the minimum occurs in the middle of nannofossil Zone NC7C, the zone underlying NC8A and a level approximately 20% of the way up from the base in the *Ticinella bejaouaensis* foraminiferal Zone (now termed the *Paraticinella rohri* Zone; Ando *et al.* 2016). Correlated to the Vocontian Basin, that level is ≈ 40 m below the Jacob Level and in the *H. nolani* ammonite Zone (see fig. 5 of Herrle and Mutterlose 2003), the zone immediately underlying the *H. jacobi* ammonite Zone.

The minimum in $^{87}Sr/^{86}Sr$ must be synchronous, so the different biostratigraphic positions of the minima show either diachroneity of the fossil datums used to calibrate the curves, or the fact that the minima are too poorly defined stratigraphically for their positions to be compared properly. As differences are small and systematic between the numerical ages of the age boundaries for the Aptian used in Bralower *et al.* (1997; 99.0, 112.2 Ma) and in GTS2020 (100.5, 113.2 Ma), these differing numerical ages cannot account for the mismatch. Evidently, much remains to be clarified with respect to the $^{87}Sr/^{86}Sr$ across the latest Aptian–earliest Albian interval.

Turning to wider issues of the temporal calibration of $^{87}Sr/^{86}Sr$ through Aptian and Albian time, the Aptian interval in Figure 1 is based on the sparse dataset of Bodin *et al.* (2015), calibrated to the ammonite zonation of the Vocontian Basin, southeastern France. Updating their trends of $^{87}Sr/^{86}Sr$ against time is made difficult by the unsettled nature of the ammonite zonations for the interval (Reboulet *et al.* 2018; Szives *et al.* 2023). Here we use the ammonite zones of GTS2020 (see their fig. 27.9) but adjust the numerical ages of a few zone boundaries in order to minimize an inflection in the late Aptian $^{87}Sr/^{86}Sr$ trend. Table 2 provides the numerical ages of the zone bases both those in GTS2020 and those of our new scale.

The biggest difference between numerical ages used here and those used in GTS2020 concerns the duration of the zone of *Acanthohoplites nolani*, which reduces from 2.4 Myr in duration in GTS2020 to 1.0 Myr here. Support for the shorter duration comes from the fact that, in GTS2020, the duration of the *A. nolani* ammonite Zone correlates to the lower 70% of the *Paraticinelli rohri* foraminiferal Zone. The duration of the P. rohri Zone is given as 3.5 Myr in GTS2020 but as 1.3 Myr in Leandro *et al.* (2022), based on cyclostratigraphic analysis of the Poggio le Guaine core, and 1.1 Myr in Charbonnier *et al.* (2023) based on cyclostratigraphic analysis of the marl-limestone alternations in the Vocontian Basin. Although these cyclostratigraphic estimates differ by 17% (and cyclostratigraphic analysis of sedimentary rocks often give rise to concern), both give shorter durations than GTS2020, so our shortening of the nolani Zone seems acceptable.

To ensure that the late Aptian minimum in $^{87}Sr/^{86}Sr$ given in the works of Bodin *et al.* (2015) and Bralower *et al.* (1997) coincide, the data of Bralower have also been reduced by 0.000018, which is the difference between the $^{87}Sr/^{86}Sr$ values of the minimum defined by each dataset. This adjustment is made on the assumption that the difference reflects either a diagenetic effect on the data of Bralower *et al.* (1997) or unnoticed interlaboratory bias, rather than the stratigraphic mismatch noted earlier.

Cenomanian, 100.5

The GSSP for the Cenomanian Stage is set at 36 m below the top of the Marnes Bleues Formation at Mont Risou, east of Rosans, Haute-Alpes, France. That level coincides with the first appearance of the planktonic foraminifera *Rotalipora globotruncanoides* Sigal, 1948 (Kennedy *et al.* 2004). There is no profile of $^{87}Sr/^{86}Sr$ through that section.

Table 2. Numerical ages and durations of ammonite zones of Barremian-to-Albian age. GTS2020 compared to this work.

Stage/age	Ammonite zone	GTS2020 Fig. 27.9 (Ma)	Duration (Myr)	This work (Ma)	Duration (Myr)	Difference in duration (Myr)
Albian	*Douvilleiceras mammillatum*	110.87	1.17	110.87	1.17	0.00
Albian	*Leymeriella tardefurcata*	111 .27	0.40	111.8	0.93	−0.53
Albian	*Leymeriella germanica*	111 .95	0.68	112.2	0.40	0.28
Albian Base	**mid *Hypacanthoplites jacobi***	**113.20**		**113.20**		
Aptian	*Hypacanthoplites jacobi*	114.40	2.45	115.00	2.80	−0.35
Aptian	*Acanthohoplites nolani*	116.80	2.40	116.00	1.00	1.40
Aptian	*Parahoplites melchioris*	117.69	0.89	116.50	0.50	0.39
Aptian	*Epicheloniceras martini*	118.76	1.07	118.40	1.90	−0.83
Aptian	*Dufrenoyia furcata*	119.15	0.39	119.15	0.75	−0.36
Aptian	*Deshayesites deshayesi*	120.00	0.85	120.40	1.25	−0.40
Aptian	*Deshayesites forbesi*	120.60	0.60	120.60	0.20	0.40
Aptian	*Deshayesites oglanlensis*	121.15	0.55	121.15	0.55	0.00
Aptian Base	**mid *Martelites sarasini***	**121.40**		**121.40**		
Barremian	*Martelites sarasini*	121.55	0.40	121.45	0.30	0.10
Barremian	*lmerites giraudi*	122.05	0.50	122.30	0.85	-0.35
Barremian	*Gerhardtia sartousi*	123.00	0.95	123.00	0.70	0.25
Barremian	*Ancyloceras vandenheckii*	124.40	1.40	124.40	1.40	0.00

The curve of $^{87}Sr/^{86}Sr$ through time for the Cenomanian is based on sparse data, so is indicative only. The foraminiferal data of Bralower *et al.* (1997) for the interval scatter a good deal and include no reliable Cenomanian data from Site 511, a site that helped define the Albian trend. Cenomanian data for the Trunch borehole, based on macrofossil fragments augmented by analysis of pre-leached bulk sediment, are too few, and the sediments too condensed, for meaningful interpretation, but appear to show values decreasing upsection through the Cenomanian-Turonian boundary (Fig. 10). The value of $^{87}Sr/^{86}Sr$ at the base of the Cenomanian section in Trunch is around 0.707 490 for a sample from the Paradoxica Bed (*Neostlingoceras carcitanensis* ammonite Subzone of the *Mantelliceras mantelli* Zone; Pearce *et al.* 2020) and approximates the value for the Albian–Cenomanian boundary, which is set at the base of the *N. carcitanensis* Sz.

In the US Western Interior, sparse data for pycnodonts, inoceramids and ammonites, through the Cenomanian (McArthur *et al.* 1994), suggest that there was little change in $^{87}Sr/^{86}Sr$ through that interval, with a decrease into the Turonian starting in the very latest Cenomanian. The base of the Cenomanian is placed at the base of the *Neogastroplites haasi* ammonite Zone and a single value for a specimen of *Texigryphe*a in the overlying zone of *Neogastoplites cornutus* has an $^{87}Sr/^{86}Sr$ value of 0.707400 $\pm$ 0.000015 (McArthur *et al.* 1994). The Cenomanian–Turonian boundary interval is poorly defined; for a discussion, see Yobo *et al.* (2021) and Ando *et al.* (2009).

Turonian, 93.9 Ma

The GSSP for the Turonian Stage is at the base of Bed 86 of the Bridge Creek Limestone Member of the Greenhorn Limestone Formation at a road-cut west of Pueblo, Colorado, USA and coincides with the first occurrence of the ammonite *Watinoceras devonense* (Kennedy *et al.* 2005). There is no $^{87}Sr/^{86}Sr$ profile through the GSSP section. In the US Western Interior, the value for $^{87}Sr/^{86}Sr$ for the base of the Turonian (base of the *Watinoceras devonense* Zone) is 0.707377 $\pm$ 0.000006 (2 s.e., $n = 10$; Fig. 11). In the Trunch borehole, the base of the Turonian is placed at 500.2 mbgl (Pearce *et al.* 2020) and the value of $^{87}Sr/^{86}Sr$ at that level, based on macrofossil debris moderated by pre-leached bulk Chalk, is around 0.707450; that is, higher than appears to be the case for the US Western Interior if these levels are indeed the same age and the samples in the Trunch borehole have not been elevated by diagenesis.

The Cenomanian–Lower Turonian interval of the Trunch section contains numerous hardgrounds and erosion surfaces (Pearce *et al.* 2020) and the age model for the borehole (Pearce *et al.* 2020) shows a pronounced change in sedimentation rate somewhere in the uppermost Turonian–lowest Cenomanian, between 460 m and 500 mbgl. Where that change occurs is not defined well, but the $^{87}Sr/^{86}Sr$ profile through the interval (Fig. 10) suggests that it might occur around 495 mbgl. There is no obvious lithological expression of such a change in the lithological log given in Pearce *et al.* (2020). The data for

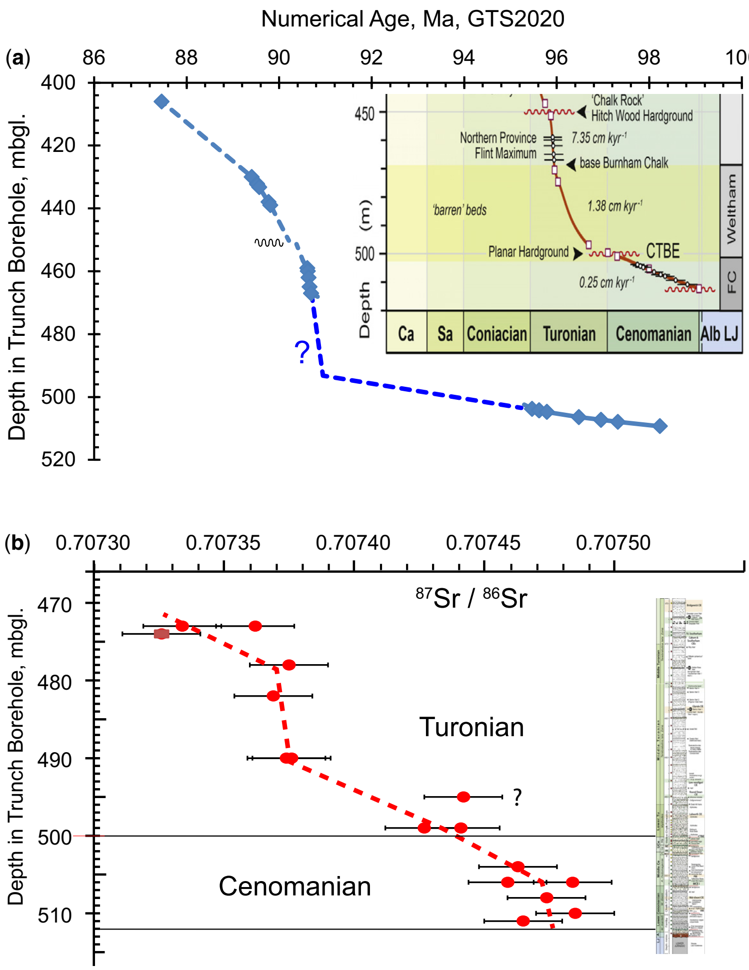

Fig. 10. (**a**) Age–depth model of Pearce *et al.* (2020) for the Trunch Borehole (inset) with the interval 470–500 mbgl reinterpreted to suggest a possible position for a change in sedimentation rate based on (**b**), which is the $^{87}Sr/^{86}Sr$ profile through that interval.

the Sr-isotope profile shown in Figure 10 scatter more than the precision of the analysis and the data are not numerous, so the $^{87}Sr/^{86}Sr$ profile in Figure 10(b) should be viewed as preliminary. Nevertheless, Figure 10 gives an idea of what might be achieved in defining levels at which sedimentation rate changes occur should more and better $^{87}Sr/^{86}Sr$ data become available.

The curve of $^{87}Sr/^{86}Sr$ against time for the Turonian is based mostly on sparse data for ammonites and inoceramids from the US Western Interior (data of McArthur *et al.* 1994); those samples could be positioned only to zonal level. Previous trends of $^{87}Sr/^{86}Sr$ through time (e.g. McArthur *et al.* 2020*b*) gave to samples a numerical age equal to the base of the zone in which the sample occurred. Here, the mid-point of the zone is used, with ages being interpolated between the ages for zone boundaries given in GTS2020. The difference this change makes to prediction of age is typically <0.5 Ma and is shown in Figure 11, where the trend through Turonian time of $^{87}Sr/^{86}Sr$ derived is compared to the trend given in McArthur *et al.* (2020*b*).

Values of $^{87}Sr/^{86}Sr$ decline through the early Turonian to a minimum in the latest Turonian before increasing again to the Turonian–Coniacian boundary. The $^{87}Sr/^{86}Sr$ value for the Turonian minimum in the US Western Interior is poorly defined by three analyses of a single inoceramid (0.707292, 0.707293, 0.707309) from the *S. whitfieldi* ammonite Zone (Table 3; McArthur *et al.* 1994). Lower values

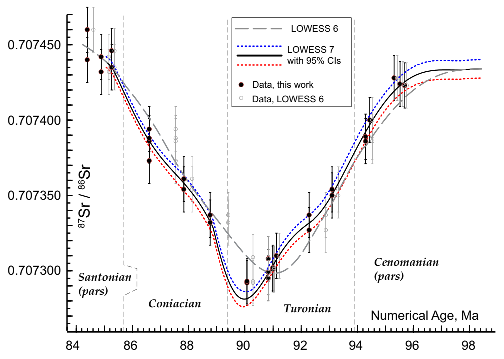

Fig. 11. Fit to the data for Turonian time derived here compared to the previous fit of McArthur *et al.* (2020*b*). Here, a minimum value of 0.707280 is modelled to occur in the *S. whitfieldi* ammonite Zone at 90.0 Ma (see text for explanation).

of 0.707280 ± 0.000003 (2 s.e., $n = 12$) are found for macrofossils from the Whisky Bay Formation of James Ross Island, Antarctica (Table 3), which is of Turonian age (Fig. 2 of Crame *et al.* 2006). Furthermore, Steuber (2001) recorded values for Turonian rudists of 0.707286 and 0.707289 (Table 3) from two sites near Salzburg, Austria. These two sets of data show either that the minimum recorded in the US Western Interior is too high by around 0.000013 (cf. analytical uncertainty of ±0.000015) because unnoticed diagenetic alteration has increased $^{87}Sr/^{86}Sr$ in the inoceramid from the *S. whitfieldi* Zone, or that the minimum lies in the unsampled latest three Turonian ammonite zones of the US Western Interior (*S.mariasensis, P. germani* and *S. nigricollensis*; Table 3). Here, it is assumed that the minimum occurs in the *S. whitfieldi* Zone and is 0.707280. Clearly, the Turonian calibration curve, as with most of the Cretaceous curve, needs improvement.

Coniacian, 89.4 ± 0.2

The GSSP for the Coniacian Stage is defined by the inoceramid bivalve species *Cremnoceramus deformis erectus* (Walaszczyk *et al.* 2022), which appears in Bed 46 of the section at Salzgitter–Salder in eastern Lower Saxony, Germany. There is no profile of $^{87}Sr/^{86}Sr$ through the section.

The curve of $^{87}Sr/^{86}Sr$ through time for the Coniacian is based in sparse data from the US Western Interior and data from the Trunch borehole (McArthur *et al.* 1993*a*, 1994). The base of the *C. d. erectus* Zone in the US Western Interior coincides with the base of the *Scaphites preventricosus* ammonite Zone (Cobban *et al.* 2006). The $^{87}Sr/^{86}Sr$ value of that level is 0.707314 ± 0.000002 (2 s.e., $n = 14$). In the Trunch borehole, *C. d. erectus* has not been found (Pearce *et al.* 2020), but those authors place the base of the Coniacian at 429.9 mbgl based on a C-isotope correlation. The lowest level in the Coniacian of the Trunch borehole for which good $^{87}Sr/^{86}Sr$ data are available is 427 mbgl. Extrapolating the $^{87}Sr/^{86}Sr$ trend to 429.9 mbgl gives a value of 0.707319 ± 0.000004 (2 s.e., $n = 8$) based on a reinterpretation of data in McArthur *et al.* (1993*a*). A lower value of 0.707293 ± 0.000006 (2 s.e.) is predicted by LOWESS 7 because of the need to accommodate a late Turonium minimum (see *Turonian* section). Further work is required to define the base Coniacian value more closely.

Santonian, 85.7 ± 0.2

The GSSP for the Santonian Stage is at 94.4 m in the eastern border of the 'Cantera de Margas' quarry, Olazagutia, Navarra, N. Spain at the first occurrence (FO) of the inoceramid bivalve *Platyceramus undulatoplicatus* (Lamolda *et al.* 2014). There is no record of $^{87}Sr/^{86}Sr$ through that section.

The base of the Santonian in the English Chalk of the Trunch borehole is at 372.5 mbgl (Lamolda *et al.* 2014; Pearce *et al.* 2020). That level is 5.5 m lower than given in McArthur *et al.* (1993*a*). The value of $^{87}Sr/^{86}Sr$ at 372.5 m is 0.707397 ± 0.000002 (2 s.e., $n = 14$). The base of the Santonian in the US Western Interior is 80% up in the *Scaphites depressus* ammonite Zone (Walaszczyk and Cobban 2007; fig. 27.9 of GTS2020), with an $^{87}Sr/^{86}Sr$ value of 0.707418 ± 0.000002 (2 s.e., $n = 6$) based on the sparse data in McArthur *et al.* (1994).

The curve for the Santonian is based on the US Western Interior, plus sparse data for the English Chalk and the Chalk of Germany (McArthur *et al.* 1993*a*, *b*, 1994), all updated to the GTS2020 timescale.

Campanian, 83.7 ± 0.5

The GSSP for the Campanian Stage is at the base of magnetic polarity Chron C33r, which occurs at 221.53 m in the Bottaccione Gorge section at Gubbio, Umbria–Marche Basin, Italy (Gale *et al.* 2023). No good record of $^{87}Sr/^{86}Sr$ exists for the section. The $^{87}Sr/^{86}Sr$ curve for the interval (Fig. 1) is based on belemnites and pre-leached bulk Chalk from Kronsmoor and Lägerdorf, northern Germany (McArthur *et al.* 1993*b*) and the assumption of a constant sedimentation rate through the sections sampled. The data of McArthur *et al.* (1993*b*) were revised for GTS2020 and here by removing a 7 m gap, assumed by those authors to be present between the top of the exposed section at Lägerdorf and the base of the exposed section in Kronsmoor,

Table 3. Turonian values of $^{87}Sr/^{86}Sr$. Values from the US Western Interior (McArthur *et al.* 1994), the Brandy Bay Member of the Whisky Bay Fm., James Ross Island, Antarctica, and Salzburg, Austria (from table 2 of Steuber 2001). For the stratigraphic levels of Antarctica samples, see Crame *et al.* (2006).

U.S. Western Interior	Ammonite Zonation (Cobban *et al.* 2006)	Type	Numeric age, GTS2020	$^{87}Sr/^{86}Sr$	±
Coniacian (Base)	*Scaphites preventricosus*	Inoceramid calcite	89.39	0.707334	15
Turonian	*Scaphites mariasensis*		89.49		
Turonian	*Prionoclycus germ ani*		89.60		
Turonian	*Scaphites nigricollensis*		89.88		
Turonian	*Scaphites whitfieldi*	Inoceramid aragonite	90.27	0.707298	15
Turonian	*Scaphites ferronensis*		90.70		
Turonian	*Scaphites warreni*	Ammonite aragonite	90.96	0.707301	15
Turonian	*Prionocyclus macombi*	*Lopha* calcite	91.03	0.707302	15
Turonian	*Prionocyclus hyatti*	Pycnodont calcite	91.22	0.707310	15
Turonian	*Collignoniceras praecox*		91.70		
Turonian	*Collignoniceras wool!gari*	Belennite calcite	92.90	0.707332	15
Turonian	*Mammites nodosoides*	*Ostrea* calcite	93.35	0.707352	15
Turonian	*Vescoceras birchbyi*		93.45		
Turonian	*Pseudapsidoceras flexuosum*		93.55		
Turonian (Base)	*Watinoceras devonense*		93.90		

Steuber (2001) Salzburg	Sample	Type	$^{87}Sr/^{86}Sr$	±
Turonian	NW24-1, St. Gilgen-Billroth	Rudist calcite	0.707292	8
Turonian	NW24-3, St. Gilgen-Billroth	Rudist calcite	0.707284	8
Turonian	NW18-1, St. Gilgen, Wolfgangsee	Rudist calcite	0.707281	8
Turonian	NW18-2, St. Gilgen, Wolfgangsee	Rudist calcite	0.707290	8

James Ross Island, Antarctica	Sample	Type	Level, m	$^{87}Sr/^{86}Sr$	±
Turonian	DJ 1456.241	Oyster	480–490	0.707277	9
Turonian	DJ 1456.236	Oyster	421.5–461.5	0.707285	9
Turonian	DJ 1456.225	Oyster	421.5–461.5	0.707279	9
Turonian	DJ 1456.217	Oyster	421.5–461.5	0.707278	9
Turonian	DJ 1456.200	Belemnite	392	0.707278	8
Turonian	DJ 1456.200	Belemnite	392	0.707287	10
Turonian	DJ 1456.199	Belemnite	392	0.707280	10
Turonian	DJ 1456187-192		392	0.707274	12
Turonian	DJ 1456181-191	Oyster	392	0.707273	10
Turonian	DJ 1456.161	Bivalve	383.5–413	0.707276	9
Turonian	DJ 1456.159	Oyster	383.5–414	0.707287	9
Turonian	DJ 1456.159	Oyster	383.5–414	0.707286	9
			Mean	0.707280	
			2 s.e.	0.000003	

following a demonstration that the gap did not exist (Voigt and Schönfeld 2010), and by expanding the section from Flint 93 to Flint 100 by 7.8 m to allow for a thickness in that interval apparently being greater than in previous lithological logs (Voigt and Schönfeld 2010).

In the US Western Interior, the base of the Campanian has been traditionally set at the base of the *Scaphites Leei* III ammonite Zone (Cobban *et al.* 2006) or some 20% up from the base (fig. 27.9 in GTS2020). The base of the zone has an $^{87}Sr/^{86}Sr$ value of 0.707454 ± 0.000002 (2 s.e., $n = 6$) based on the data of McArthur *et al.* (1994); the value for the base of the overlying zone of *Scaphites hippocrepis I* is 0.707465. Thibault *et al.* (2016; their figs 9 and 10) correlate the base of the *S. leei* III Zone to the level of the last occurrence of the crinoid *Marsupites testudinarius* in the English Chalk.

In the English Chalk, the traditional placement of the base of the Campanian has been the last occurrence of the crinoid *Marsupites testudinarius* (e.g. discussion in Gale *et al.* 2023). The $^{87}Sr/^{86}Sr$ value for that level in the Chalk of the Trunch Borehole (307.4 mbgl; Pearce *et al.* 2020) is 0.707477 ± 0.000001 (2 s.e., $n = 30$) based on reinterpretation of the data of McArthur *et al.* (1993*a*). The base of Chron 33r is suggested by Jarvis *et al.* (2023) to occur at 294 mbgl in the Trunch borehole; that level has an $^{87}Sr/^{86}Sr$ value of 0.707490 ± 0.000004 ($n = 34$). Montgomery *et al.* (1998) place the base of Chron 33r in the lower part of the *Gonioteuthis granulata/Socialis uintercrinus* Zone. In the Trunch borehole, that level (assumed to be 20% up in the zone) has an $^{87}Sr/^{86}Sr$ value of 0.707450 ± 0.000001 (2 s.e., $n = 30$).

In the Chalk of Germany at Lägerdorf, the traditional placement of the base of the Campanian has been the base of the *Gonioteuthis granulataquadrata* belemnite Zone (Schulz *et al.* 1984; Schönfeld *et al.* 1996), for which the value of $^{87}Sr/^{86}Sr$ is 0.707460 ± 0.000001 (2 s.e., $n = 16$), based on a reinterpretation of the data of McArthur *et al.* (1993*b*). According to Jarvis *et al.* (2023, fig. 14), the base of Chron 33r should be some 20 m higher and at the base of the *Offaster pilula* Zone in Lägerdorf. This level coincides with a prominent market horizon, marl M1, and has an $^{87}Sr/^{86}Sr$ value of 0.707482 ± 0.000001 (2 s.e., $n = 16$). At Lägerdorf, Thibault *et al.* (2016, their fig. 5) appear to place the boundary (base of Chron 33r) within the lowermost part of the *Offaster pilula* Zone, so the base of Chron 33r in Lägerdorf on that placement would have a value greater than 0.707482. If the level of Chron 33r in the English Chalk given by Montgomery *et al.* (1998) is correlated biostratigraphically to be 20% up in the *U. socialis* Zone of Lägerdorf, the level would be around 16 m below that for which $^{87}Sr/^{86}Sr$ data exist; the $^{87}Sr/^{86}Sr$ value for that level can be estimated by extrapolation to be around 0.707430.

The values of boundaries given above provide guidance in correlating boundary levels from place to place. Given the increased understanding of all aspects of SIS gained over the past few decades, and the refinement of the stratigraphy of the Chalk of Germany in that period, it is clear that dedicated profiling anew of $^{87}Sr/^{86}Sr$ across the Santonian–Campanian boundary (or any other boundary), using analysis of macrofossils and the most modern instrumentation, would prove more than capable of resolving the discrepancies alluded to above. Until then, we can interpret only the data to hand, and in doing so have retained in LOWESS 7 the traditional placements of the base of the Campanian in the Chalk of northwestern Europe until further work definitively establishes the level of the base of Chron 33r in sections suitable for defining $^{87}Sr/^{86}Sr$ of the boundary.

Maastrichtian (72.2 ± 0.2) and the Maastrichtian–Danian Boundary, 66.04

The GSSP for the Maastrichtian Stage is defined as a mean position of 12 fossil datums at Tercis les Bains, in southwestern France (Odin and Lamaurelle 2001). No $^{87}Sr/^{86}Sr$ profile exists for the section.

The most detailed boundary profile of $^{87}Sr/^{86}Sr$ is that of McArthur *et al.* (1993*b*) for belemnites and pre-leached bulk Chalk from Kronsmoor, northern Germany. Correlations from the GSSP place the base of the Maastrichtian in Kronsmoor either 14 m above the prominent stratigraphic marker bed labelled Flint 600 (see fig. 4 of Voigt and Schönfeld 2010) or 12.5 m above Flint 600 at the level of marl mB609 (see fig. 2 of Wilmsen *et al.* 2019). The latter is within a few metres of the base of the *Belemnella obtusa* belemnite Zone, which is taken in GTS 2020 as the base of the Maastrichtian. The $^{87}Sr/^{86}Sr$ values are 0.707744 ± 0.000002 (2 s.e., $n = 21$) for the 12.5 m level and 0.707746 ± 0.000002 (2 s.e., $n = 21$) for the 14 m level. In Voigt *et al.* (2012) and in GTS2020, the boundary correlates to the uppermost *Baculites eliasi* ammonite Zone of the US Western Interior, which has an $^{87}Sr/^{86}Sr$ value of around 0.707739, based on extrapolation from adjacent zones of the data of McArthur *et al.* (1994).

In the borehole at Trunch, the base of the Maastrichtian was set around a level 61 mbgl by Wood *et al.* (1994). That level has an $^{87}Sr/^{86}Sr$ value of 0.707729 ± 0.000005 (2 s.e., $n = 9$). According to Voigt *et al.* (2012), C-isotope stratigraphy shows that the base of the Maastrichtian is not present in the borehole; nevertheless, their figure 5 suggests that, were it present, it would be around 40 mbgl, a level 7 m above the highest sample analysed. The 40 m level would, by extrapolation, have an $^{87}Sr/^{86}Sr$ value of 0.707758 ± 0.000005 (2 s.e., $n = 9$).

Updating the Maastrichtian curve of $^{87}Sr/^{86}Sr$ against time for Figure 1 used the $^{87}Sr/^{86}Sr$ data of Barrera *et al.* (1997) for DSDP Site 463 fitted to the age model of Li and Keller (1999), plus the data from Sugarman *et al.* (1995) from the Atlantic coastal plain of New Jersey, USA, and (for the lower Maastrichtian) data from McArthur *et al.* (1993*b*) from the German Chalk at Kronsmoor. The trend so defined has a value of 0.707744 ± 0.000003 (95% CI) for the base of the Maastrichtian.

The value for $^{87}Sr/^{86}Sr$ at the base of the Danian is fixed by the data of McArthur *et al.* (1998) for the Maastrichtian–Danian boundary as being 0.707830 ± 0.000006 (2 s.e., $n = 76$) based on macrofossil debris from sections on Seymour Island, Antarctica (0.707832 ± 0.000005; 2 s.e., $n = 43$) and pre-leached bulk Chalk from Kjølby Gaard and Nye Kløv, Denmark (0.707828 ± 0.000003; 2 s.e., $n = 33$). The boundary in neither section is marked by any anomaly in $^{87}Sr/^{86}Sr$.

Competing interests The authors declare that they have no known competing financial interests or personal relationships that could have appeared to influence the work reported in this paper.

Author contributions **JMM**: conceptualization (equal), data curation (lead), formal analysis (equal), investigation (lead), project administration (lead), writing – original draft (lead), writing – review & editing (lead); **RJH**: formal analysis (equal), writing – original draft (supporting).

Funding This research received no specific grant from any funding agency in the public, commercial, or not-for-profit sectors.

Data availability The Phanerozoic Sr-isotope curve, LOWESS 7, which includes the updated Cretaceous Sr-isotope curve, is available on ResearchGate and from JM McArthur via e-mail at j.mcarthur@ucl.ac.uk

References

Ager, D.V. 1973. *The Nature of the Stratigraphical Record*. Wiley, New York.

Ager, D.V. 1993. *The Nature of the Stratigraphical Record*, 3rd edn. Wiley, Chichester.

Allison, N. 1996. Comparative determinations of trace and minor elements in coral aragonite by ion microprobe analysis, with preliminary results from Phuket, southern Thailand. *Geochimica et Cosmochimica Acta*, **60**, 3457–3470, https://doi.org/10.1016/0016-7037(96)00171-8

Andersson, P.S., Wasserburg, C.J. and Ingri, J. 1992. The sources and transport of Sr and Nd isotopes in the Baltic Sea. *Earth and Planetary Science Letters*, **113**, 459–472, https://doi.org/10.1016/0012-821X(92)90124-E

Ando, A., Nakano, T., Kaiho, K., Kobayashi, T., Kokado, E. and Khim, B.-K. 2009. Onset of seawater $^{87}Sr/^{86}Sr$ excursion prior to Cenomanian–Turonian oceanic anoxic event 2? New late Cretaceous strontium isotope curve from the central Pacific Ocean. *Journal of Forestry Research*, **39**, 322–334, https://doi.org/10.2113/gsjfr.39.4.322

Ando, A., Nakano, T., Kawahata, H., Yokoyama, Y. and Khim, B-K. 2010. Testing seawater Sr isotopic variability on a glacial-interglacial timescale: an application of latest high-precision thermal ionization mass spectrometry. *Geochemical Journal*, **44**, 347–357.

Ando, A., Huber, B.T. and Premoli Silva, I. 2016. Paraticinella rohri (Bolli, 1959) as the valid name for the latest Aptian zonal marker species of planktonic foraminifera traditionally called bejaouaensis or eubejaouaensis. *Cretaceous Research*, **45**, 275–287, https://doi.org/10.1016/j.cretres.2013.05.002

Bailey, R. 2023. Cyclostratigraphy at a tipping point. *Geology Today*, **39**, 99–106.

Bailey, R.J. and Smith, D.G. 2008*a*. Discussion on the Late Palaeocene–Early Eocene and Toarcian (Early Jurassic) carbon isotope excursions: a comparison of their time scales, associated environmental change, causes and consequences (*Journal of the Geological Society of London*, Vol. 164, 2007, 1093–1108). *Journal of the Geological Society of London*, **165**, 875–880, https://doi.org/10.1144/0016-76492007-157

Bailey, R.J. and Smith, D.G. 2008*b*. Quantitative tests for stratigraphic cyclicity. *Geological Journal*, **43**, 431–446, https://doi.org/10.1002/gj.1115

Bailey, T.R., McArthur, J.M., Prince, H. and Thirlwall, M.F. 2000. Dissolution methods for strontium isotope stratigraphy: whole rock analysis. *Chemical Geology*, **167**, 313–319, https://doi.org/10.1016/S0009-2541(99)00235-1

Barbin, V., Ramseyer, K., Debenay, J.P., Schein, E., Roux, M. and Decrouez, D. 1991. Cathodoluminescence of Recent biogenic carbonates: an environmental and ontogenetic fingerprint. *Geological Magazine*, **128**, 19–26, https://doi.org/10.1017/S001675680001801X

Barefoot, E.A., Nittrouer, J.A. and Straub, K.M. 2023. Sedimentary processes and the temporal resolution of sedimentary strata. *Geophysical Research Letters*, **50**, e2023GL103925, https://doi.org/10.1029/2023GL103925

Barrera, E., Savin, S., Thomas, E. and Jones, C.E. 1997. Evidence for thermohaline-circulation reversals controlled by sea-level change in the latest Cretaceous. *Geology*, **25**, 715–718, https://doi.org/10.1130/0091-7613(1997)025<0715:EFTCRC>2.3.CO;2

Bodin, S., Meissner, P., Janssen, N.M.M., Steuber, S. and Mutterlose, J. 2015. Large igneous provinces and organic carbon burial: controls on global temperature and continental weathering during the Early Cretaceous. *Global and Planetary Change*, **133**, 238–253, https://doi.org/10.1016/j.gloplacha.2015.09.001

Bralower, T.J., Fullagar, P.D., Paull, C.K., Dwyer, G.S. and Leckie, R.M. 1997. Mid-Cretaceous strontium-isotope stratigraphy of deep-sea sections. *Geological Society of America Bulletin*, **109**, 1421–1442, https://doi.org/10.1130/0016-7606(1997)109<1421:MCSISO>2.3.CO;2

Brand, U. and Veizer, J. 1980. Chemical diagenesis of a multicomponent carbonate system: 1. Trace elements. *Journal of Sedimentary Petrology*, **50**, 1219–1236.

Brand, U. and Veizer, J. 1981. Chemical diagenesis of a multicomponent carbonate system: 2. Stable isotopes. *Journal of Sedimentary Petrology*, **51**, 987–997.

Bryant, J.D., Jones, D.S. and Mueller, P.A. 1995. Influence of freshwater flux on $^{87}Sr/^{86}Sr$ chronostratigraphy in marginal marine environments and dating of vertebrate and invertebrate faunas. *Journal of Paleontology*, **69**, 1–6, https://doi.org/10.1017/S002233600002686X

Burke, W.H., Denison, R.E., Hetherington, E.A., Koepnick, R.B., Nelson, H.F. and Otto, J.B. 1982. Variation of $^{87}Sr/^{86}Sr$ throughout Phanerozoic time. *Geology*, **10**, 516–519, https://doi.org/10.1130/0091-7613(1982)10<516:VOSSTP>2.0.CO;2

Burla, S., Oberli, F., Heimhofer, U., Wiechert, U. and Weissert, H. 2009. Improved time control on Cretaceous coastal deposits: new results from Sr isotope measurements using laser ablation. *Terra Nova*, **21**, 401–409, https://doi.org/10.1111/j.1365-3121.2009.00897.x

Charbonnier, G., Boulila, S., Spangenberg, J.E., Vermeulen, J. and Galbrun, B. 2023. Astrochronology of the Aptian Stage and evidence for the chaotic orbital motion of Mercury. *Earth and Planetary Science Letters*, **610**, 118104, https://doi.org/10.1016/j.epsl.2023.118104

Cobban, W.A., Walaszczyk, I., Obradovich, J.D. and McKinney, K.C. 2006. *A USGS zonal table for the Upper Cretaceous middle Cenomanian–Maastrichtian of the Western Interior of the United States based on ammonites, inoceramids, and radiometric ages*. U.S. Geological Survey Open–File Report, **2006-1250**.

Coogan, L.A. and Dosso, S.E. 2015. Alteration of ocean crust provides a strong temperature dependent feedback on the geological carbon cycle and is a primary driver of the Sr-isotopic composition of seawater. *Earth and Planetary Science Letters*, **415**, 38–46, https://doi.org/10.1016/j.epsl.2015.01.027

Crame, J.A., Pirrie, D. and Riding, J.B. 2006. Mid-Cretaceous stratigraphy of the James Ross Basin, Antarctica. *Geological Society, London, Special Publications*, **258**, 7–19, https://doi.org/10.1144/GSL.SP.2006.258.01.02

Dasch, D.J. and Biscaye, P.E. 1971. Isotopic composition of Cretaceous-to-Recent pelagic foraminifera. *Earth and Planetary Science Letters*, **11**, 201–204, https://doi.org/10.1016/0012-821X(71)90164-6

Denison, R.E. and Peryt, T.M. 2009. Strontium isotopes in the Zechstein (Upper Permian) an hydrites of Poland: evidence of varied meteoric contributions to marine brines. *Geological Quarterly*, **53**, 159–166, https://gq.pgi.gov.pl/article/view/7510/0

Denison, R.E., Kirkland, D.W. and Evans, R. 1998. Using strontium isotopes to determine the age and origin of gypsum and anhydrite beds. *Journal of Geology*, **106**, 1–17, https://doi.org/10.1086/515996

Denison, R.E., Miller, N.R., Scott, R.W. and Reaser, D.F. 2003. Strontium isotope stratigraphy of the Comanchean Series in north Texas and southern Oklahoma. *Geological Society of America Bulletin*, **115**, 669–682, https://doi.org/10.1130/0016-7606(2003)115<0669:SISOTC>2.0.CO;2

Diehl, A. and Bach, W. 2023. MARHYS Database 3.0. PANGAEA, https://doi.org/10.1594/PANGAEA.958978

Dudás, F.Ö., Yuan, D.X., Shen, S.Z. and Bowring, S.A. 2017. A conodont-based revision of the $^{87}Sr/^{86}Sr$ seawater curve across the Permian-Triassic boundary. *Palaeogeography, Palaeoclimatology, Palaeoecology*, **470**, 40–53, https://doi.org/10.1016/j.palaeo.2017.01.007

Dummann, W., Steinig, S. *et al*. 2020. The impact of Early Cretaceous gateway evolution on ocean circulation and organic carbon burial in the emerging South Atlantic and Southern Ocean basins. *Earth and Planetary Science Letters*, **530**, 115890, https://doi.org/10.1016/j.epsl.2019.115890

El Meknassi, S., Dera, G., Cardone, T., De Rafélis, M., Brahmi, C. and Chavagnac, V. 2018. Sr isotope ratios of modern carbonate shells: good and bad news for chemostratigraphy. *Geology*, **46**, 1003–1006, https://doi.org/10.1130/G45380.1

Farrell, J.W., Clemens, S.C. and Gromet, L.P. 1995. Improved chronostratigraphic reference curve of late Neogene seawater $^{87}Sr/^{86}Sr$. *Geology*, **23**, 403406.

Farkaš, J., Frýda, J. *et al*. 2018. Chromium isotope fractionation between modern seawater and biogenic carbonates from the Great Barrier Reef, Australia: implications for the paleo-seawater δ^{53}Cr reconstruction. *Earth and Planetary Science Letters*, **498**, 140–151.

Gale, A.S., Montgomery, P., Kennedy, W.J., Hancock, J.M., Burnett, J.A. and McArthur, J.M. 1995. Definition and global correlation of the Santonian-Campanian boundary. *Terra Nova*, **7**, 611–622, https://doi.org/10.1111/j.1365-3121.1995.tb00710.x

Gale, A., Batenburg, S. *et al*. 2023. The Global Boundary Stratotype Section and Point (GSSP) of the Campanian Stage at Bottaccione (Gubbio, Italy) and its Auxiliary Sections: Seaford Head (UK), Bocieniec (Poland), Postalm (Austria), Smoky Hill, Kansas (U.S.A), Tepayac (Mexico). *Episodes*, 46, 451–490, https://doi.org/10.18814/epiiugs/2022/022048

Goldstein, S.J. and Jacobsen, S. 1987. The Nd and Sr isotopic systematics of river-water dissolved material: implications for the sources of Nd and Sr in seawater. *Chemical Geology*, **66**, 245–272.

Gradstein, F.M., Ogg, J.G. and Smith, A.G. (eds) 2004. *A Geologic Timescale 2004*. CUP.

Gradstein, F.M., Ogg, J.G., Schmitz, M.D. and Ogg, G.M. 2020. *A Geologic Time Scale 2020*. Elsevier.

Henderson, G.M., Martel, D.J., O'Nions, R.K. and Shackleton, N.J. 1994. Evolution of seawater $^{87}Sr/^{86}Sr$ over the last 400 ka: the absence of glacial/interglacial cycles. *Earth Planetary Science Letters*, **128**, 643–651.

Herrle, J.O. and Mutterlose, J. 2003. Calcareous nannofossils from the Aptian–Lower Albian of southeast France: palaeoecological and biostratigraphic implications. *Cretaceous Research*, **24**, 1–22, https://doi.org/10.1016/S0195-6671(03)00023-5

Hildreth, R.A. and Henderson, W.T. 1971. Comparison of $^{87}Sr/^{87}Sr$ for sea-water strontium and the Eimer and Amend $SrCO_3$. *Geochimica et Cosmochimica Acta*, **35**, 235–238, https://doi.org/10.1016/0016-7037(71)90061-5

Hodell, D.A., Mead, G.A. and Mueller, P.A. 1990. Variation in the strontium isotopic composition of seawater (8 Ma to present): implications for chemical weathering rates and dissolved fluxes to the oceans. *Chemical Geology (Isotope Geoscience Section)*, **80**, 291–307.

Huang, C., Hinnov, L., Fischer, A.G., Grippo, A. and Herbert, T. 2010. Astronomical tuning of the Aptian Stage from Italian reference sections. *Geology*, **38**, 899–902, https://doi.org/10.1130/G31177.1

Huber, B.T., MacLeod, K.G. and Tur, N.A. 2008. Chronostratigraphic framework for Upper Campanian – Maastrichtian sediments on the Blake Nose (subtropical North Atlantic). *Journal of Foraminiferal Research*, **38**, 162–182, https://doi.org/10.2113/gsjfr.38.2.162

Ingram, B.L. and Sloan, D. 1992. Strontium isotopic composition of estuarine sediments as paleosalinity-paleoclimate indicator. *Science (New York, NY)*, **255**, 68–72, https://doi.org/10.1126/science.255.5040.68

ICS 2023. International Commission on Stratigraphy, https://stratigraphy.org/gssps/

Jarvis, I., Pearce, M.A. *et al*. 2023. Carbon isotopes, palynology and stratigraphy of the Santonian–Campanian boundary: the GSSP auxiliary sections, Seaford Head (England) and Bocieniec (Poland), and correlation between the Boreal and Tethyan realms. *Cretaceous*

Research, **143**, 105415, https://doi.org/10.1016/j.cretres.2022.105415

Jenkyns, H.C., Paull, C.K., Cummins, D.I. and Fullagar, P.D. 1995. Strontium-isotope stratigraphy of Lower Cretaceous atoll carbonates in the Mid-Pacific Mountains. *In*: Winterer, E.L., Sager, W.W., Firth, J.V. and Sinton, J.M. (eds) *Proceedings of the Ocean Drilling Program, Scientific Results*, **143**, 89–97

Jones, C.E., Jenkyns, H.C., Coe, A.L. and Hesselbo, S.P. 1994*a*. Strontium isotope variations in Jurassic and Cretaceous seawater. *Geochimica et Cosmochimica Acta*, **58**, 3061–3074, https://doi.org/10.1016/0016-7037(94)90179-1

Jones, C.E., Jenkyns, H.C. and Hesselbo, S.P. 1994*b*. Strontium isotopes in Early Jurassic seawater. *Geochimica et Cosmochimica Acta*, **58**, 1285–1301, https://doi.org/10.1016/0016-7037(94)90382-4

Kiel, S., Glodny, J. *et al*. 2014. The paleoecology, habitats, and stratigraphic range of the enigmatic Cretaceous brachiopod *Peregrinella*. *PLoS ONE*, **9**, e109260, https://doi.org/10.1371/journal.pone.0109260

Kenjo, S., Reboulet, S., Mattioli, E. and Ma'louleh, K. 2021. The BerriasianeValanginian boundary in the Mediterranean Province of the Tethyan Realm: ammonite and calcareous nannofossil biostratigraphy of the Vergol section (Montbrun-les-Bains, SE France), candidate for the Valanginian GSSP. *Cretaceous Research*, **121**, 104738, https://doi.org/10.1016/j.cretres.2020.104738

Kennedy, W.J., Gale, A.S., Bown, P.R., Caron, M., Davey, R.J., Gröcke, D. and Wray, D.S. 2000. Integrated stratigraphy across the Aptian–Albian boundary in the Marnes Bleues, at the Col de Pré-Guittard, Arnayon (Dröme), and at Tartonne (Alpes-de-Haute-Provence), France: a candidate Global Boundary Stratotype Section and Boundary Point for the base of the Albian Stage. *Cretaceous Research*, **21**, 591–720.

Kennedy, W.J., Gale, A.S., Lees, J.A. and Caron, M. 2004. The Global Boundary Stratotype Section and Point (GSSP) for the base of the Cenomanian Stage, Mont Risou, Hautes-Alpes, France. *Episodes*, **27**, 21–32, https://doi.org/10.18814/epiiugs/2004/v27i1/003

Kennedy, W.J., Walaszczyk, I. and Cobban, W.A. 2005. The Global Boundary Stratotype Section and Point for the base of the Turonian Stage of the Cretaceous: Pueblo, Colorado, USA. *Episodes*, **28**, 93–104, https://doi.org/10.18814/epiiugs/2005/v28i2/003

Kennedy, J.W., Gale, A.S., Huber, B.T., Petrizzo, M.R., Bown, P. and Jenkyns, H.C. 2017. The Global Boundary Stratotype Section and Point (GSSP) for the base of the Albian Stage, of the Cretaceous, the Col de Pré-Guittard section, Arnayon, Drôme, France. *Episodes*, **40**, 177–188, https://doi.org/10.18814/epiiugs/2017/v40i3/017021

Koepnick, R.B., Burke, W.H., Denison, R.E., Hetherington, E.A., Nelson, H.F., Otto, J.B. and Waite, L E. 1985. Construction of the seawater $^{87}Sr/^{86}Sr$ curve for the Cenozoic and Cretaceous: supporting data. *Chemical Geology (Isotope Geoscience Section)*, **58**, 55–81, https://doi.org/10.1016/0168-9622(85)90027-2

Krabbenhöft, A., Fietzke, J., Eisenhauer, A., Liebetrau, V., Böhm, F. and Vollstaedt, H. 2009. Determination of radiogenic and stable strontium isotope ratios ($^{87}Sr/^{86}Sr$; $\delta^{88}/^{86}Sr$) by thermal ionization mass spectrometry applying an $^{87}Sr/^{84}Sr$ double spike. *Journal of Analytical Atomic Spectrometry*, **24**, 1267–1271, https://doi.org/10.1039/b906292k

Kuznetsov, A.B., Semikhatov, M.A. and Gorokhov, I.M. 2012. The Sr isotope composition of the world ocean, marginal and inland seas: implications for the Sr isotope stratigraphy. *Stratigraphy and Geological Correlation*, **20**, 501–515, https://doi.org/10.1134/S0869593812060044

Kuznetsov, A.B., Izokh, O.P., Dzyuba, O.S. and Shurygin, B.N. 2017. Sr isotope composition in belemnites from the Jurassic–Cretaceous boundary section (Maurynya River, Western Siberia). *Doklady Earth Sciences*, **477**, 1408–1413, https://doi.org/10.1134/S1028334X17120029

Kuznetsov, A.B., Semikhatov, M.A. and Gorokhov, I.M. 2018. Strontium isotope stratigraphy: principles and state of the art. *Stratigraphy and Geological Correlation*, **26**, 367–386, https://doi.org/10.1134/S0869593818040056

Lamolda, M.A., Paul, C.R.C., Peryt, D. and Pons, J.M. 2014. The Global Boundary Stratotype and Section Point (GSSP) for the base of the Santonian Stage, 'Cantera de Margas', Olazagutia, northern Spain. *Episodes*, **37**, 2–13, https://doi.org/10.18814/epiiugs/2014/v37i1/001

Leandro, C.G., Savian, J.F. *et al*. 2022. Astronomical tuning of the Aptian Stage and its implications for age recalibrations and paleoclimatic events. *Nature Communications*, **13**, 2941, https://doi.org/10.1038/s41467-022-30075-3

Li, L.-Q. and Keller, G. 1999. Variability in Late Cretaceous climate and deep waters: evidence from stable isotopes. *Marine Geology*, **161**, 171–190, https://doi.org/10.1016/S0025-3227(99)00078-X

Li, Q., McArthur, J.M. *et al*. 2021. Testing with $\delta^{44/40}Ca$ and $\delta^{88/86}Sr$ for ocean acidification during the Early Toarcian. *Chemical Geology*, **574**, 120228, https://doi.org/10.1016/j.chemgeo.2021.120228

MacLeod, K.G., Fullagar, P.D. and Huber, B.T. 2003. $^{87}Sr/^{86}Sr$ test of the degree of impact-induced slope failure in the Maastrichtian of the western North Atlantic. *Geology*, **31**, 311–314, https://doi.org/10.1130/0091-7613(2003)031<0311:SSTOTD>2.0.CO;2

Marshall, J.D. 1988. *Cathodoluminescence of Geological Materials*. Unwin Hyman, Boston.

Martin, E.E. and Scher, H.D. 2004. Preservation of seawater Sr and Nd isotopes in fossil fish teeth: bad news and good news. *Earth and Planetary Science Letters*, **220**, 25–39, https://doi.org/10.1016/S0012-821X(04)00030-5

Martinez, M., Deconinck, J.F., Pellenard, P., Reboulet, S. and Riquier, L. 2013. Astrochronology of the Valanginian Stage from reference sections (Vocontian Basin, France) and palaeoenvironmental implications for the Weissert Event. *Palaeogeography, Palaeoclimatology, Palaeoecology*, **376**, 91–102, https://doi.org/10.1016/j.palaeo.2013.02.021

Martinez, M., Deconinck, J.F., Pellenard, P., Riquier, L., Company, M., Reboulet, S. and Moiroud, M. 2015. Astrochronology of the Valanginian–Hauterivian Stages (Early Cretaceous): chronological relationships between the Parana–Etendeka large igneous province and the Weissert and the Faraoni events. *Cretaceous*

Research, **131**, 158–173, https://doi.org/10.1016/j.gloplacha.2015.06.001

Matsui, H., Horikawa, K. *et al*. 2019. Integrated Neogene biochemostratigraphy at DSDP Site 296 on the Kyushu–Palau Ridge in the western North Pacific. *Newsletters on Stratigraphy*, **53**, 313–331, https://doi.org/10.1127/nos/2019/0549

McArthur, J.M. 1994. Recent trends in strontium isotope stratigraphy. *Terra Nova*, **6**, 331–358, https://doi.org/10.1111/j.1365-3121.1994.tb00507.x

McArthur, J.M. 2010. Strontium isotope stratigraphy. In: Application of Modern Stratigraphic Techniques: Theory and Case Histories. *In*: Ratcliffe, K.T. and Zaitlin, B.A. (eds) *SEPM Special Publication No. 94. SEPM (Society for Sedimentary Geology)*, 129–142.

McArthur, J.M. and Howarth, R.J. 2004. Strontium isotope stratigraphy. *In*: Gradstein, F.M., Ogg, J.G. and Smith, A.G. (eds) *A Geologic Timescale 2004*. CUP, 1 plate.

McArthur, J.M., Thirlwall, M.F., Gale, A.S., Kennedy, W.J., Burnett, J.A. and Mattey Lord, A.R. 1993*a*. Strontium isotope stratigraphy for the Late Cretaceous: a new curve, based on the English Chalk. *Geological Society, London, Special Publications*, **70**, 195–209, https://doi.org/10.1144/GSL.SP.1993.070.01.14

McArthur, J.M., Chen, M., Gale, A.S., Thirlwall, M.F. and Kennedy, W.J. 1993*b*. Strontium isotope stratigraphy for the Late Cretaceous: age models and intercontinental correlations for the Campanian. *Paleoceanography*, **8**, 859–873, https://doi.org/10.1029/93PA02324

McArthur, J.M., Kennedy, W.J., Chen, M., Thirlwall, M.F. and Gale, A.S. 1994. Strontium isotope stratigraphy for the Late Cretaceous: direct numerical age calibration of the Sr-isotope curve for the U.S. Western Interior Seaway. *Palaeogeography, Palaeoclimatology, Palaeoecology*, **108**, 95–119, https://doi.org/10.1016/0031-0182(94)90024-8

McArthur, J.M., Thirlwall, M.F., Engkilde, M., Zinsmeister, W.J. and Howarth, R.J. 1998. Strontium isotope profiles across K/T boundaries in Denmark and Antarctica. *Earth and Planetary Science Letters*, **160**, 179–192, https://doi.org/10.1016/S0012-821X(98)00058-2

McArthur, J.M., Donovan, D.T., Thirlwall, M.F., Fouke, B.W. and Mattey, D. 2000. Strontium isotope profile of the Early Toarcian (Jurassic) Oceanic Anoxic Event, the duration of ammonite biozones, and belemnite palaeotemperatures. *Earth and Planetary Science Letters*, **179**, 269–285, https://doi.org/10.1016/S0012-821X(00)00111-4

McArthur, J.M., Mutterlose, J., Price, G.D., Rawson, P.F., Ruffell, A. and Thirlwall, M.F. 2004. Belemnites of Valanginian, Hauterivian and Barremian age: Sr-isotope stratigraphy, composition ($^{87}Sr/^{86}Sr$, $\delta^{13}C$, $\delta^{18}O$, Na, Sr, Mg) and palaeo-oceanography. *Palaeogeography, Palaeoclimatology, Palaeoecology*, **202**, 253–272, https://doi.org/10.1016/S0031-0182(03)00638-2

McArthur, J.M., Janssen, N.M.M., Reboulet, S., Leng, M.J., Thirlwall, M.F. and van de Schootbrugge, B. 2007. Palaeotemperatures, polar ice-volume, and isotope stratigraphy (Mg/Ca, $\delta^{18}O$, $\delta^{13}C$, $^{87}Sr/^{86}Sr$): the Early Cretaceous (Berriasian, Valanginian, Hauterivian). *Palaeogeography, Palaeoclimatology, Palaeoecology*, **248**, 391–430, https://doi.org/10.1016/j.palaeo.2006.12.015

McArthur, J.M., Steuber, T., Page, K.N. and Landman, N.H. 2016. Sr-isotope stratigraphy: assigning time in the Campanian, Pliensbachian, Toarcian, and Valanginian. *Journal of Geology*, **145**, 569–586, https://doi.org/10.1086/687395

McArthur, J.M., Page, K., Duarte, L.V., Thirlwall, M.F., Li, Q., Weis, R. and Comas-Rengifo, M.J. 2020*a*. Sr-isotope stratigraphy ($^{87}Sr/^{86}Sr$) of the lowermost Toarcian of Peniche, Portugal, and its relation to ammonite zonations. *Newsletters on Stratigraphy*, **53**, 297–312, https://doi.org/10.1127/nos/2019/0492

McArthur, J.M., Howarth, R.J., Shields, G.A. and Zhou, Y. 2020*b*. Chapter 7: Strontium isotope stratigraphy. *In*: Gradstein, F.M., Ogg, J.G., Schmitz, M.D. and Ogg, G.M. (eds) *A Geologic Time Scale 2020*. Elsevier, **1**, 211–238.

Mokadem, F., Parkinson, I.J., Hathorne, E.C., Ananda, P., Allen, J.T. and Burton, K.W. 2015, High-precision radiogenic strontium isotope measurements of the modern and glacial ocean: limits on glacial–interglacial variations in continental weathering. *Earth and Planetary Science Letters*, **415**, 111–120, https://doi.org/10.1016/j.epsl.2015.01.036

Möller, C., Mutterlose, J. and Alsen, P. 2015. Integrated stratigraphy of Lower Cretaceous sediments (Ryazanian–Hauterivian) from North-East Greenland. *Palaeogeography, Palaeoclimatology, Palaeoecology*, **437**, 85–97, https://doi.org/10.1016/j.palaeo.2015.07.014

Montgomery, P., Hailwood, E.A., Gale, A.S. and Burnett, J.A. 1998. The magnetostratigraphy of Coniacian–Late Campanian chalk sequences in southern England. *Earth and Planetary Science Letters*, **156**, 209–224, https://doi.org/10.1016/S0012-821X(98)00008-9

Mutterlose, J., Rawson, P.F. and Reboulet, S. 2021. The Global Boundary Stratotype Section and Point (GSSP) for the base of the Hauterivian Stage (Lower Cretaceous), La Charce, southeast France. *Episodes*, **44**, 129–150, https://doi.org/10.18814/epiiugs/2020/020072

Odin, G.S. and Lamaurelle, M.A. 2001. The global Campanian-Maastrichtian Stage boundary. *Episodes*, **24**, 229–238, https://doi.org/10.18814/epiiugs/2001/v24i4/002

Oyanagi, R., Okamoto, A., Satish-Kumar, M., Minami, M., Harigane, Y. and Michibayashi, K. 2021. Hadal aragonite records venting of stagnant paleoseawater in the hydrated forearc mantle. *Communications Earth & Environment*, **2**, 243, https://doi.org/10.1038/s43247-021-00317-1

Palmer, M.R. and Edmond, J.M. 1989. The strontium isotope budget of the modern ocean. *Earth and Planetary Science Letters*, **92**, 11–26, https://doi.org/10.1016/0012-821X(89)90017-4

Paces, J.B., Minor, S.A., Schmidt, K.M. and Hoffmann, J. 2023. *Strontium isotope chronostratigraphic age of a sirenian fossil site on Santa Rosa Island, Channel Islands National Park, California*. U.S. Geological Survey Scientific Investigations Report, **2023-5026**.

Pearce, C.R., Parkinson, I.J., Gaillardet, J., Charlier, B.L.A., Mokadem, F. and Burton, K.W. 2015. Reassessing the stable ($\delta^{88}/^{86}Sr$) and radiogenic ($^{87}Sr/^{86}Sr$) strontium isotopic composition of marine inputs. *Geochimica et Cosmochimica Acta*, **157**, 125–146, https://doi.org/10.1016/j.gca.2015.02.029

Pearce, M.A., Jarvis, I., Ball, P.J. and Laurin, J. 2020. Palynology of the Cenomanian to lowermost Campanian (Upper Cretaceous) Chalk of the Trunch Borehole (Norfolk, UK) and a new dinoflagellate cyst bioevent stratigraphy for NW Europe. *Review of Palaeobotany and Palynology*, **278**, 104188, https://doi.org/10.1016/j.revpalbo.2020.104188

Peterman, Z.E., Hedge, C.E. and Tourtelot, H.A. 1970. Isotopic composition of strontium in sea water throughout Phanerozoic time. *Geochimica et Cosmochimica Acta*, **34**, 105–120, https://doi.org/10.1016/0016-7037(70)90154-7

Peucker-Ehrenbrink, B. 2009. Land2Sea database of river drainage basin sizes, annual water discharges and suspended sediment fluxes. *Geochemistry, Geophysics, Geosystems*, **10**, Q06014, https://doi.org/10.1029/2008GC002356

Peucker-Ehrenbrink, B. 2018. Land2Sea Database, Version 2.0. Pangaea, https://doi.org/10.1594/PANGAEA.892680

Peucker-Ehrenbrink, B. and Fiske, G.J. 2019. A continental perspective of the seawater $^{87}Sr/^{86}Sr$ record: a review. *Chemical Geology*, **510**, 140–165, https://doi.org/10.1016/j.chemgeo.2019.01.017

Podlaha, O.G., Mutterlose, J. and Veizer, J. 1998. Preservation of $\delta^{18}O$ and $\delta^{13}C$ in belemnite rostra from the Jurassic/Early Cretaceous successions. *American Journal of Science*, **298**, 324–347, https://doi.org/10.2475/ajs.298.4.324

Prokoph, A., Shields, G.A. and Veizer, J. 2008. Compilation and time-series analysis of a marine carbonate $\delta^{18}O$, $\delta^{13}C$, $^{87}Sr/^{86}Sr$ and $\delta^{34}S$ database through Earth history. *Earth-Science Reviews*, **87**, 113–133, https://doi.org/10.1016/j.earscirev.2007.12.003

Rawson, P. 1971. The Hauterivian (Lower Cretaceous) biostratigraphy of the Speeton Clay of Yorkshire, England. *Newsletters on Stratigraphy*, **1**, 61–76, https://doi.org/10.1127/nos/1/1971/61

Reboulet, S., Szives, O. *et al*. 2018. Report on the 6th International Meeting of the IUGS Lower Cretaceous Ammonite Working Group, the Kilian Group (Vienna, Austria, 20th August 2017). *Cretaceous Research*, **91**, 100e110, https://doi.org/10.1016/j.cretres.2018.05.008

Reboulet, S. Adatte, T. *et al*. 2023. The Global Boundary Stratotype Section and Point (GSSP) for the base of the Valanginian Stage (Lower Cretaceous): the informal proposal of the Vergol candidate section (Drôme, southeast France). *In prep* for ICS, July 2023.

Roth, P.H. 1978. Cretaceous nannoplankton biostratigraphy and oceanography of the northwestern Atlantic Ocean. *In*: Benson, W.E., Sheridan, R.E. *et al*. (eds) *Initial Reports of the Deep Sea Drilling Project*, **44**, 731–759, https://doi.org/10.2973/dsdp.proc.44.134.1978

Ruebsam, W., Münzberger, P. and Schwark, L. 2014. Chronology of the Early Toarcian environmental crisis in the Lorraine Sub-basin (NE Paris Basin). *Earth and Planetary Science Letters*, **404**, 273–282, https://doi.org/10.1016/j.epsl.2014.08.005

Ruebsam, W., Münzberger, P. and Schwark, L. 2015. Reply to the comment by Boulila and Hinnov towards 'Chronology of the Early Toarcian environmental crisis in the Lorraine Sub-basin (NE Paris Basin)' by W. Ruebsam, P. Münzberger, and L. Schwark [*Earth Planet. Sci Letters*, 404, 273–282]. *Earth and Planetary Science Letters*, **416**, 147–150, https://doi.org/10.1016/j.epsl.2015.02.022

Sadler, P.M. 1981. Sediment accumulation rates and the completeness of stratigraphic sections. *The Journal of Geology*, **89**, 569–584, https://doi.org/10.1086/628623

Schönfeld, J., Schulz, M.-G. *et al*. 1996. New results on biostratigraphy, palaeomagnetics, geochemistry and correlation from the standard section for the Upper Cretaceous White Chalk of northern Germany. *Mitteilungen aus dem Geologisch-Paläontologischen Institut der Universität Hamburg*, **7**, 545–575.

Schulz, M.-G., Ernst, G., Ernst, H. and Schmid, F. 1984. Coniacian to Maastrichtian Stage boundaries in the standard section for the Upper Cretaceous white chalk of NW Germany (Lägerdorf-Kronsmoor-Hemmoor): Definitions and proposals. *Bulletin of the Geological Society of Denmark*, **33**, 203–215, https://doi.org/10.37570/bgsd-1984-33-19

Smalley, P.C., Higgins, A.C., Howarth, R.J., Nicholson, H., Jones, C.E., Swinburne, N.H.M. and Bessa, J. 1994. Seawater Sr isotope variations through time: a procedure for constructing a reference curve to date and correlate marine sedimentary rocks. *Geology*, **22**, 431–343, https://doi.org/10.1130/0091-7613(1994)022<0431:SSIVTT>2.3.CO;2

Smith, D.G. 2023. The Orbital Cycle Factory: Sixty cyclostratigraphic spectra in need of re-evaluation. *Palaeogeography, Palaeoclimatology, Palaeoecolology*, **628**, 111744.

Speight, J.G. (ed.) 2017. *Lange's Handbook of Chemistry*, 17th edn. McGraw-Hill Education, New York, https://www.accessengineeringlibrary.com/content/book/9781259586095

Spooner, E.T.C. 1976. The strontium isotopic composition of seawater, and seawater-oceanic crust interaction. *Earth and Planetary Science Letters*, **31**, 167–174, https://doi.org/10.1016/0012-821X(76)90108-4

Steuber, T. 2001. Strontium isotope stratigraphy of Turonian–Campanian Gosau-type rudist formations in the Northern Calcareous and Central Alps (Austria and Germany). *Cretaceous Research*, **22**, 429–441, https://doi.org/10.1006/cres.2001.0268

Sugarman, P.J., Miller, K.G., Bukry, D. and Feigenson, M.D. 1995. Uppermost Campanian-Maastrichtian strontium isotopic, biostratigraphic, and sequence stratigraphic framework of the new Jersey Coastal Plain. *Geological Society of America Bulletin*, **107**, 19–37, https://doi.org/10.1130/0016-7606(1995)107<0019:UCMSIB>2.3.CO;2

Szives, O., Latil, J.-L., Moreno-Bedmar, J.A., Lehmann, J., Robert, E. and Owen, H.G. 2023. Critical revision and new proposals on the Aptian–Albian zonation of the Standard Mediterranean Ammonite Zonal Scheme. *Newsletters on Stratigraphy*, **56**, 423–456, https://doi.org/10.1127/nos/2023/0753

Thibault, N., Jarvis, I., Voigt, S., Gale, A.S., Attree, K. and Jenkyns, H.C. 2016. Astronomical calibration and global correlation of the Santonian (Cretaceous) based on the marine carbon isotope record. *Paleoceanography*, **31**, 847–865, https://doi.org/10.1002/2016PA002941

Thirlwall, M.F. 1991. Long-term reproducibility of multi-collector Sr and Nd isotope ratio analysis. *Chemical Geology (Isotope Geoscience Section)*, **94**, 85–104, https://doi.org/10.1016/0168-9622(91)90002-E

Vaughan, S., Bailey, R.J. and Smith, D.G. 2011. Detecting cycles in stratigraphic data: spectral analysis in the presence of red noise. *Paleoceanography*, **26**, PA4211, https://doi.org/10.1029/2011PA002195

Vaughan, S., Bailey, R.J. and Smith, D.G. 2014. Cyclostratigraphy: data filtering as a source of spurious spectral peaks. *Geological Society, London, Special Publications*, **404**, 151–156, https://doi.org/10.1144/SP404.11

Veizer, J. 1989. Strontium isotopes in seawater through time. *Annual Review of Earth and Planetary Sciences*, **17**, 141–167, https://doi.org/10.1146/annurev.ea.17.050189.001041

Veizer, J., Buhl, D. *et al*. 1997. Strontium isotope stratigraphy: potential resolution and event correlation. *Palaeogeography, Palaeoclimatology, Palaeoecology*, **132**, 65–77, https://doi.org/10.1016/S0031-0182(97)00054-0

Veizer, J. and Compston, W. 1974. $^{87}Sr/^{86}Sr$ composition of seawater during the Phanerozoic. *Geochimica et Cosmochimica Acta*, **33**, 1461–1484.

Veizer, J., Ala, D. *et al*. 1999. $^{87}Sr/^{86}Sr$, $\delta^{13}C$ and $\delta^{18}O$ evolution of Phanerozoic seawater. *Chemical Geology*, **161**, 59–88, https://doi.org/10.1016/S0009-2541(99)00081-9

Voigt, S. and Schönfeld, J. 2010. Cyclostratigraphy of the reference section for the Cretaceous white chalk of northern Germany, Lägerdorf–Kronsmoor: a late Campanian–early Maastrichtian orbital time scale. *Palaeogeography, Palaeoclimatology, Palaeoecology*, **287**, 67–80, https://doi.org/10.1016/j.palaeo.2010.01.017

Voigt, S., Gale, A.S., Jung, C. and Jenkyns, H.C. 2012. Global correlation of Upper Campanian–Maastrichtian successions using carbon-isotope stratigraphy: development of a new Maastrichtian timescale. *Newsletters on Stratigraphy*, **45**, 25–53, https://doi.org/10.1127/0078-0421/2012/0016

Voigt, J., Hathorne, E.C., Frank, M., Vollstaedt, H. and Eisenhauer, A. 2015. Variability of carbonate diagenesis in equatorial Pacific sediments deduced from radiogenic and stable Sr isotopes. *Geochimica et Cosmochimica Acta*, **148**, 360–377.

Vollstaedt, H., Eisenhauer, A. *et al*. 2014. The Phanerozoic $\delta^{88}/^{86}Sr$ record of seawater: new constraints on past changes in oceanic carbonate fluxes. *Geochimica et Cosmochimica Acta*, **128**, 249–265, https://doi.org/10.1016/j.gca.2013.10.006

Walaszczyk, I. and Cobban, W.A. 2007. Inoceramid fauna and biostratigraphy of the upper Middle Coniacian–lower Middle Santonian of the Pueblo Section (SE Colorado, U.S. Western Interior). *Cretaceous Research*, **28**, 132–142, https://doi.org/10.1016/j.cretres.2006.05.024

Walaszczyk, I., Čech, S. *et al*. 2022. The Global Boundary Stratotype Section and Point (GSSP) for the base of the Coniacian Stage (Salzgitter-Salder, Germany) and its auxiliary sections (Słupia Nadbrzeżna, central Poland; Střeleč, Czech Republic; and El Rosario, NE Mexico). *Episodes*, **45**, 181–220, https://doi.org/10.18814/epiiugs/2021/021022

Weedon, 2022. Problems with the current practice of spectral analysis in cyclostratigraphy: avoiding false detection of regular cyclicity. *Earth Science Reviews*, **235**, 104261.

Westerhold, T. and 23 Others. 2020. An astronomically dated record of Earth's climate and its predictability over the last 66 million years. *Science (New York, NY)*, **369**, 1383, https://doi.org/10.1126/science.aba6853

Wierzbowski, H., Anczkiewicz, R., Pawlak, J., Rogov, M.A. and Kuznetsov, A.B. 2017. Revised Middle–Upper Jurassic strontium isotope stratigraphy. *Chemical Geology*, **466**, 239–255, https://doi.org/10.1016/j.chemgeo.2017.06.015

Wickman, F.E. 1948. A clue to the age of certain marine sediments. *Journal of Geology*, **56**, 61–66, https://doi.org/10.1086/625478

Wilmsen, M., Engelke, J., Linnert, C., Mutterlose, J. and Niebuhr, B. 2019. A Boreal reference section revisited (Kronsmoor, northern Germany): high-resolution stratigraphic calibration of the Campanian – Maastrichtian boundary interval (Upper Cetaceous). *Newsletters on Stratigraphy*, **52**, 155–172, https://doi.org/10.1127/nos/2018/0473

Wood, C.J., Morter, A.A. and Gallois, R.W. 1994. Appendix 1: upper cretaceous stratigraphy of the Trunch Borehole (TG23SE/8). *In*: Arthurton, R.S., Booth, S.J. *et al*. (eds) *Geology of the country around Great Yarmouth*. Memoir of the British Geological Survey, Sheet 162 (England and Wales).

Yobo, L.N., Brandon, A.D., Holmden, C., Lau, K.V. and Eldrett, J. 2021. Changing inputs of continental and submarine weathering sources of Sr to the oceans during OAE 2. *Geochimica et Cosmochimica Acta*, **303**, 205–222, https://doi.org/10.1016/j.gca.2021.03.013

Zaky, A.H., Brand, U. *et al*. 2019. Strontium isotope geochemistry of modern and ancient archives: tracer of secular change in ocean chemistry. *Canadian Journal of Earth Sciences*, **56**, 245–264, https://doi.org/10.1139/cjes-2018-0085